JCI The Journal of Clinical Investigation

An endothelial SOX18-mevalonate pathway axis enables repurposing of statins for infantile hemangioma

Annegret Holm, … , Mathias Francois, Joyce Bischoff

J Clin Invest. 2025. https://doi.org/10.1172/JCI179782.

Research In-Press Preview Angiogenesis Vascular biology

Graphical abstract

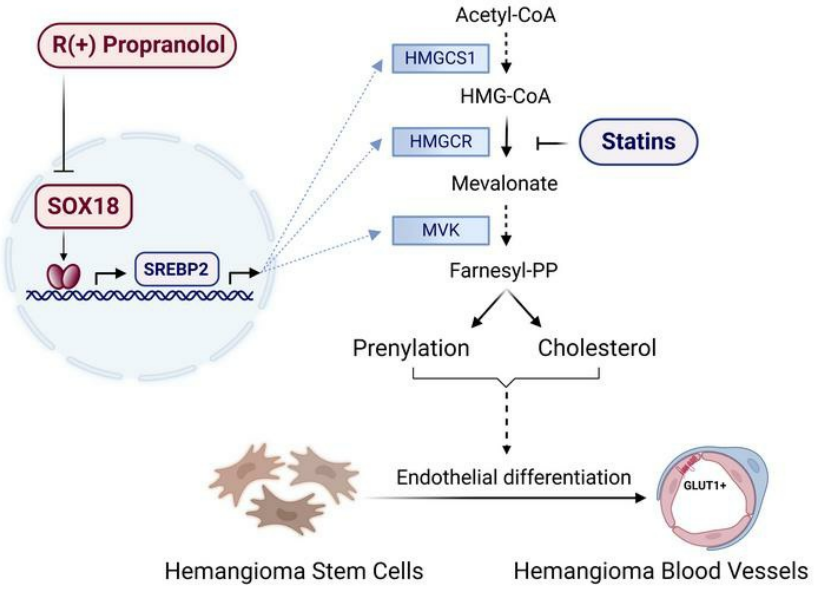

An endothelial SOX18-mevalonate pathway axis enables repurposing of statins for infantile hemangioma

Annegret Holm[1], Matthew S. Graus[2], Jill Wylie-Sears[1], Jerry Wei Heng Tan[1#], Maya Alvarez-Harmon[1], Luke Borgelt[1], Sana Nasim[1], Long Chung[2], Ashish Jain[3], Mingwei Sun[3], Liang Sun[3], Pascal Brouillard[4], Ramrada Lekwuttikarn[5], Yanfei Qi[2], Joyce Teng[5], Miikka Vikkula[4,6], Harry Kozakewich[7], John B. Mulliken[8], Mathias Francois[2,9], and Joyce Bischoff[1*]

Affiliations:

[1] Vascular Biology Program, Department of Surgery, Boston Children's Hospital, Harvard Medical School, Boston, MA, United States.
[2] The David Richmond Laboratory for Cardiovascular Development: Gene Regulation and Editing, The Centenary Institute, The University of Sydney, Camperdown, New South Wales, Australia.
[3] Research Computing, Information Technology, Boston Children's Hospital, Boston, United States.
[4] Human Molecular Genetics, de Duve Institute, University of Louvain, Brussels, Belgium; VASCERN-VASCA European Reference Center.
[5] Department of Dermatology, Lucile Packard Children' Hospital at the Stanford University School of Medicine, Palo Alto, California.
[6] WELBIO Department, WEL Research Institute, Wavre, Belgium.
[7] Department of Pathology, Boston Children's Hospital, Harvard Medical School, Boston, MA, United States.
[8] Department of Plastic and Oral Surgery, Boston Children's Hospital; Department of Surgery, Harvard Medical School, Boston, United States.
[9] School of Biomedical Sciences, The University of Sidney, Camperdown, New South Wales, Australia.

*Address correspondence to:

Joyce Bischoff, PhD
Boston Children's Hospital
300 Longwood Ave, Boston, MA 02115
Phone: 617-919-2192
Email: joyce.bischoff@childrens.harvard.edu

current address: Graduate School of Biomedical Sciences, University of Texas Southwestern Medical Center, Dallas, Texas

ABSTRACT:

Infantile hemangioma (IH) is the most common tumor in children and a paradigm for pathological vasculogenesis, angiogenesis, and regression. Propranolol, the mainstay treatment, inhibits IH vessel formation via a β-adrenergic receptor independent off-target effect of its R(+) enantiomer on the endothelial SRY box transcription factor 18 (SOX18). Transcriptomic profiling of patient-derived hemangioma stem cells (HemSC) uncovered the mevalonate pathway (MVP) as a target of R(+) propranolol. Loss and gain of function of SOX18 confirmed it is both necessary and sufficient for R(+) propranolol suppression of the MVP, including regulation of sterol regulatory element binding protein 2 (SREBP2) and the rate-limiting enzyme HMG-CoA reductase (HMGCR). A biological relevance of the endothelial SOX18-MVP axis in IH patient tissue was demonstrated by nuclear co-localization of SOX18 and SREBP2. Functional validation in a preclinical IH xenograft model revealed that statins – competitive inhibitors of HMGCR – efficiently suppress IH vessel formation. We propose an endothelial SOX18-MVP-axis as a central regulator of IH pathogenesis and suggest statin repurposing to treat IH. The pleiotropic effects of R(+) propranolol and statins along the SOX18-MVP axis to disable an endothelial-specific program may have therapeutic implications for other vascular disease entities involving pathological vasculogenesis and angiogenesis.

Word count: 195

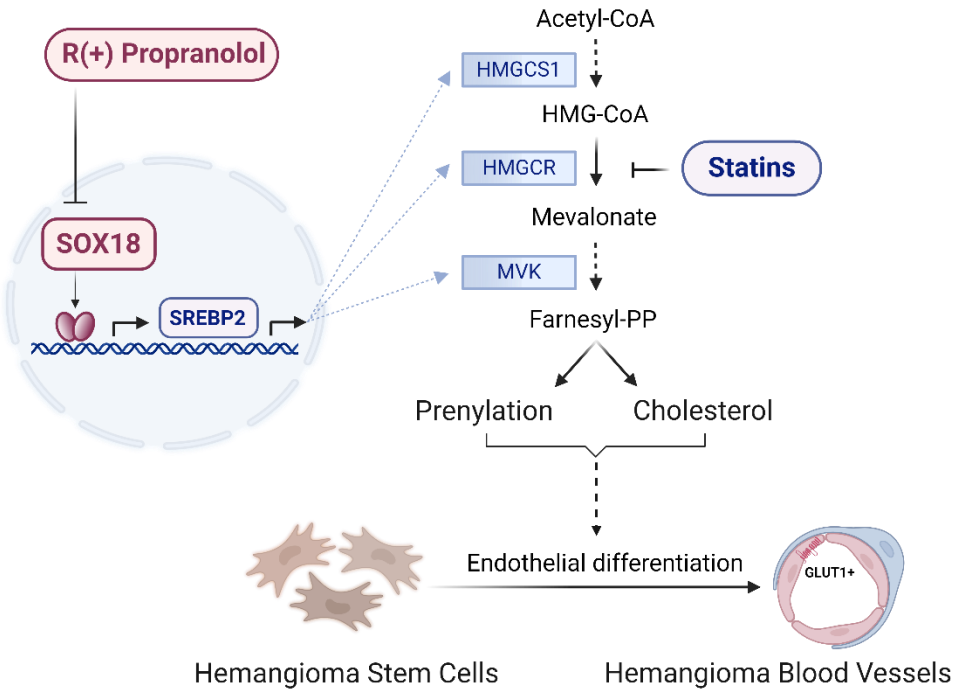

52

53 **Graphical abstract**

INTRODUCTION:

Infantile hemangioma (IH) is a benign vascular tumor of infancy with an incidence of 2-10%. It predominantly occurs in female and premature infants of European descent. IH arises postnatally at 2-7 weeks of age with rapid neovascularization during the proliferating phase, which can continue for 4-18 months of age. A spontaneous and gradual involuting phase follows, spanning 3-9 years. A subset of IH - termed rebounding or regrowing IH - does not undergo complete involution and may regrow after treatment discontinuation. The underlying cellular mechanism of IH formation is the differentiation of multipotent hemangioma stem cells (HemSC) into hemangioma endothelial cells (HemEC) and hemangioma pericytes to form neo vessels (vasculogenesis), concurrent with cellular proliferation (1-4). For most children, IH poses no serious risk; however, 10-15% of lesions require treatment to prevent sequelae such as disfigurement, functional impairment including vision loss and airway obstruction, consumptive hypothyroidism, and high-output cardiac failure (5). Propranolol was discovered serendipitously to be effective for IH; it is currently the only FDA-approved drug for IH(6). Despite successful repurposing for IH, propranolol is associated with beta-adrenergic side effects including hypotension, bradycardia, peripheral vasospasm, bronchospasm, hypoglycemia and seizures, sleep disturbance, and potentially adverse neurocognitive outcomes (6-10). The complete response rate to propranolol is reported to be 60% (6). These safety and efficacy concerns underscore the need for additional treatments for IH. Therapeutic avenues have remained limited due to a lack of information on the molecular basis of propranolol mode of action in IH.

Propranolol acts as a non-selective antagonist of β1-and β2-adrenergic receptors GPCRs; it is a 1:1 mixture of S(-) and R(+) enantiomers. The S(-) enantiomer is a potent antagonist of β1 and β2-adrenergic receptors, while the R(+) enantiomer is largely devoid of beta-blocker activity (11). This provided an opportunity to identify a R(+) propranolol-dependent pathway in hemangioma stem cells (HemSC)(12, 13). HemSC are isolated from proliferating phase IH specimens, are mesenchymal in nature, exhibit multilineage differentiation potential, and have been shown to recapitulate hemangiogenesis in nude mice (2). R(+) propranolol inhibits HemSC endothelial differentiation in vitro and HemSC vasculogenesis in a pre-clinical IH model (12, 13). Furthermore, we established that R(+) propranolol interferes directly with the activity of the transcription factor SRY (sex-determining region Y) HMG box-containing 18 (SOX18). In addition to propranolol, pharmacological interference with SOX18 is achieved through use of the small molecule inhibitor Sm4 (14), which provided further validation of the role of SOX18 in IH (12, 13). These findings have led to the repurposing of propranolol in patients with hypotrichosis-

lymphedema-telangiectasia-renal defect syndrome (HLTRS) - a rare vascular disease caused by a dominant-negative truncating mutation in SOX18 (15). These observations provided evidence for the pharmaco-genetic interaction between SOX18 and propranolol in a vascular disease (12). In summary, we identified a SOX18-dependent inhibition of HemSC endothelial differentiation and vessel formation in vivo as the molecular basis of propranolol-mediated inhibition of vessel formation in IH.

SOX18 is a master transcriptional regulator of vascular development and endothelial specification and is expressed in nascent blood and lymphatic endothelium as well as in endothelial progenitor cells (16). It plays fundamental roles in arterial specification, lymphangiogenesis and angiogenesis (17) and in tumor angiogenesis (18). Its known role in instructing the molecular program of endothelial specification and differentiation prompted us to investigate the role of SOX18 in the context of HemSC endothelial differentiation.

In this study, we set out to identify genes whose expression in differentiating HemSC is altered by R(+) propranolol-mediated inhibition of SOX18. We discovered that R(+) propranolol rapidly downregulates transcripts encoding enzymes in the mevalonate pathway (MVP) in a SOX18 dependent manner. The MVP is central to cholesterol and isoprenoid biosynthesis and is controlled by the rate-limiting enzyme HMGCoA reductase A (HMGCR) (19), which produces mevalonate. A critical regulator of MVP genes is the transcription factor SREBP2 (20).

We show statins, competitive HMGCR inhibitors, potently reduce blood vessel formation in a preclinical IH model. Statins are widely prescribed to reduce LDL cholesterol in patients at risk for cardiovascular disease (21). As a consequence of inhibiting the MVP, statins increase LDL receptor expression, thereby enhancing clearance of LDL cholesterol from the bloodstream. Here, we uncover a molecular relationship between the endothelial-specific transcription factor SOX18 and the MVP. We demonstrate R(+) propranolol downregulates MVP genes in HemSC during their endothelial differentiation. In vitro, using loss and gain of function-based approaches, we show SOX18 is necessary and sufficient for R(+) propranolol-mediated regulation of the MVP. We propose SOX18 may act as a rheostat of the MVP in pathological endothelium, and we determine that this axis is critical to IH disease progression. Blocking the MVP with statins inhibits HemSC endothelial differentiation and vessel formation, suggesting that statins could be repurposed to treat IH.

RESULTS:

R(+) propranolol-induced SOX18 inhibition reduces MVP gene expression during HemSC endothelial differentiation.

To identify the downstream targets of R(+) propranolol in HemSC to endothelial cell (HemEC) differentiation, we performed bulk RNA sequencing of HemSC isolated from 6 different IH specimens. Table 1 provides an overview of patient samples used in respective experiments. HemSC were induced to undergo endothelial differentiation for 6 days (2) and then treated with or without R(+) propranolol (20 uM) for 2 hours (Supplemental Figure 1.1). HemSC at Day 4 of endothelial differentiation, prior to onset of endothelial marker expression, were treated with R(+) propranolol and analyzed as well. The timing and dose of R(+) propranolol were determined by previously observed downregulation of *NOTCH1* expression, a SOX18 transcriptional target (13). Endothelial differentiation of HemSC was validated by increased relative gene expression in SOX18 and VE-Cadherin over the course of 6 days (Supplemental Figure 1.2).

The Kyoto Encyclopedia of Genes and Genomes (KEGG) analysis identified steroid biosynthesis as differentially affected on Day 6. This was confirmed by gene ontology analysis of the subontology *biological processes*, with most of the top terms related to cholesterol or isoprenoid biosynthesis and processes involved in angiogenesis (Figure 1A; Supplemental Table 1). Figure 1B shows a heatmap of differentially expressed MVP genes as well as genes in cholesterol and isoprenoid biosynthesis on Day 4 and Day 6. Gene by gene analysis revealed R(+) propranolol treatment on Day 6 significantly reduced transcripts encoding several enzymes of the MVP, including the rate-limiting enzyme HMGCR as well HMGCS1 and mevalonate kinase (MVK), while few changes were seen at Day 4 (Figure 1B, C and Supplemental Table 1). Of note, ABCA1 - a negative regulator of the MVP(22) - was upregulated at Day 6. Overall, 107 genes in HemSC were differentially expressed at Day 4 versus 2482 genes at Day 6 of differentiation (Figure 1C). Differential expression was defined as Log_2 fold change >1 and adjusted p-value <0.05. Comparative analysis of the time points defines a window for SOX18 inhibition using R(+) propranolol, supported by the lack of downregulation of MVP transcripts at Day 4 of differentiation, where relatively low endothelial marker and SOX18 expression was seen (Figure 1D, Supplemental Table 1, Supplemental Figure 1.2). The significant increase in *SOX18* mRNA from Day 4 to Day 6 of endothelial differentiation is consistent with the onset of MVP gene sensitivity to R(+) propranolol at Day 6 (Figure 1D). Downregulation of *HMGCS1*, *HMGCR*, and *MVK* was confirmed by qPCR in cells treated with R(+) propranolol for 2 hours or continuously for 4 days of the endothelial differentiation protocol (Figure 1E).

To further elucidate the effect of SOX18 inhibition on the MVP, we investigated SOX18-binding locations in the genome using a publicly available ChIP-Seq dataset in HUVEC (23). We discovered SOX18 binding sites within the *HMGCS1* and *HMGCR* gene loci that corresponded with ENCODE-defined cis-regulatory elements (Figure 2A). R(+) propranolol-induced changes in gene expression, combined with the identification of SOX18-binding sites in regulatory regions of *HMGCS1* and *HMGCR*, support the possibility that interference of SOX18 activity may perturb transcriptional regulation of critical genes along the MVP pathway.

***SOX18 gain and loss of function confirms its role as an endothelial fine tuner of MVP genes*.**

To interrogate the role of SOX18 in regulating the MVP, we used gain of function (lentiviral overexpression) and gene depletion (shRNA knockdown) in HemSC and HemEC, respectively. SOX18 overexpression (OE) in undifferentiated HemSC resulted in a significant increase in the mRNA levels of *HMGCS1, HMGCR, MVK,* and *NOTCH1* (Figure 2B). The known SOX18 target, *NOTCH1*, served as a positive control for SOX18 transcriptional activity. R(+) propranolol reduced expression of all four genes in HemSC^{SOX18OE} (Figure 2C). This demonstrates that SOX18 is sufficient to drive the MVP in HemSC. We next knocked down SOX18 in HemEC that express high levels of SOX18. mRNA levels of *HMGCS1*, *HMGCR*, *MVK*, and *NOTCH1* in control HemEC were significantly reduced by R(+) propranolol (Figure 2D), as seen in HemSC undergoing endothelial differentiation (Figure 1E). SOX18 knockdown abolished the R(+) propranolol effect on expression of *HMGCS1, HMGCR, MVK,* and *NOTCH1* in HemEC^{shSOX18} (Figure 2E). This demonstrates that SOX18 is needed to increase MVP gene expression in HemEC. In summary, these experiments demonstrate via genetic manipulation that SOX18 is both necessary and sufficient to regulate the transcription of MVP genes and to mediate the pharmacological effect of R(+) propranolol on the MVP.

SOX18 positively regulates MVP biosynthetic output in human endothelial cells.

To validate the role of SOX18 in regulating genes in the MVP, we tested whether disruption of SOX18 activity with R(+) propranolol or the SOX18 small molecule inhibitor Sm4 (14) would have an effect on cholesterol biosynthesis in HUVEC. First, HUVEC were depleted of cholesterol by incubation with methyl beta-cyclodextrin (MBCD) and treated ± R(+) propranolol or ± Sm4 for 16 hours, allowing for new cholesterol synthesis to take place, which was then measured by targeted mass spectrometry. Endogenous cholesterol levels were significantly reduced in R(+) propranolol- and Sm4-treated HUVEC,

consistent with SOX18-mediated downregulation of MVP gene expression (Figure 3A,B). We also tested the effect of an overexpressed, dominant negative version of SOX18 (*Ragged Opossum* (*RaOp*) that is known to disrupt SOX18 activity(24). Using FACS as a readout, we determined that SOX18^{RaOp} expression decreased HMGCS1 and HMGCR protein levels compared to its wild-type control on a cell population scale (Figure 3C,D; Supplemental Figure 3.1). This indicates an effect on two key MVP enzymes that control this pathway. Both experiments demonstrate that SOX18 positively regulates cholesterol biosynthesis in an endothelial context.

R(+) propranolol mode of action on the MVP is mediated via a SOX18-/SREBP2-dependent mechanism.

SREBP2 is the master transcriptional regulator of MVP genes and is ubiquitously expressed(20). Based on the above findings, we posit that in HemSC undergoing endothelial differentiation, SOX18 coordinates with SREBP2. To test this, we analyzed the effect of R(+) propranolol on levels of the precursor SREBP2 (122 kDa), which resides in the endoplasmic reticulum, as well as mature SREBP2 (62kDa) - the basic helix loop helix (bHLH) leucine zipper domain(20, 25). When endogenous cholesterol levels drop, the inactive 122 kDa precursor is transported to the Golgi and proteolytically cleaved to release the active 62kDa mature form. The latter translocates into the nucleus to activate transcription of MVP genes (Figure 3E). We hypothesized that R(+) propranolol would reduce 62 kDa SREBP2 in HemSC undergoing endothelial differentiation. HemSC (n=4) were treated for 2 hours ± R(+) propranolol on Day 6 of endothelial differentiation. Cell lysates analyzed by Western Blot (WB) showed the R(+) propranolol treatment decreased mature 62kDa SREBP2 (Figure 3F,G). Rapid turnover of mature SREBP2 within 4 hours has been demonstrated (26). The reduced levels of 62 kDa SREBP2 upon R(+) propranolol treatment are consistent with the bulk RNA-Seq and qPCR data and suggest SOX18 increases SREBP2 maturation, thereby influencing the MVP output. The anti-human SREBP2 antibody used to detect precursor and mature forms of SREBP2 was validated in MBCD cholesterol depleted HemSC (Supplemental Figure 3.2).

We next assessed SOX18-dependency of the R(+) propranolol mediated effects on SREBP2 in gain of function and gene depletion experiments as in Figure 2B-E. We assessed the effect of SOX18 overexpression in HemSC on SREBP2, its chaperone sterol regulatory element binding protein cleavage-activating protein (SCAP), and its cleavage proteins site 1 protease (S1P) and site 2 protease (S2P) (20). Indeed, overexpressed SOX18 in HemSC resulted in significantly increased *SREBP2*, *SCAP*, *S1P*, and *S2P* mRNA levels, which was abolished by R(+) propranolol (Figure 3H,J). Knockdown of SOX18 in HemEC had the opposite effect: mRNA levels of *SREBP2*, *SCAP*, and *S1P* were significantly reduced; *S2P* was reduced

but not significantly (Figure 3I,K). Immunofluorescence staining of control HemEC and HemEC ^{shSOX18} confirmed the efficient knockdown of SOX18 and a corresponding decrease in SREBP2 (Figure 3L,M), consistent with the reduced SREBP2 transcript level in the HemEC^{shSOX18} (Figure 3I). WB analyses of SREBP2 are consistent with these results (Supplemental Figures 3.3 and 3.4). SOX18 OE in undifferentiated HemSC resulted in significantly increased 62 kDa SREBP2 (Supplemental Figure 3.3). In control HemEC, an increase in 62kDa of SREBP2 was observed upon R(+) propranolol treatment, likely due to feedback mechanisms over the 24-hour treatment period (26). Importantly, SOX18 knockdown in HemEC abolished the effect of R(+) propranolol on levels of the 62kDa SREBP2 (Supplemental Figure 3.4). Together, these data suggest that SOX18 increases transcript levels of SREBP2 itself and the genes needed for processing SREBP2 to its active form. We speculate SOX18 may provide a boost to isoprenoid biosynthesis in differentiating, nascent endothelium by increasing expression of *HMGCS1, HMGCR*, as suggested in Figure 2A, and *SREBP2, SCAP, SIP, S2P* as shown here.

Nuclear SOX18 and SREBP2 in proliferating phase and regrowing IH indicate active MVP.

We investigated the nuclear localization of SOX18 and SREBP2 in histological sections from proliferating, involuting, and regrowing IH (Figure 4). We stained proliferating and involuting IH tissue sections (n=10, each) from specimens excised from patients with IH who had not been treated with propranolol or corticosteroid (or any other treatment). Immunofluorescent staining of SOX18, SREBP2, and with the lectin *Ulex Europaeus Agglutinin I* (UEA1), which specifically binds to human endothelial cells, showed co-localization of SOX18 and SREBP2 in endothelial nuclei throughout proliferating phase IH sections (Figure 4A-D, Supplemental Figure 4.2). SOX18 was largely absent in involuting phase IH. Age-matched human skin (n=4), stained in parallel for comparison, was devoid of SOX18. SOX18 is not routinely detected in mature, quiescent blood vessels, as it is not needed to maintain an endothelial phenotype (27). We quantified SOX18^{+}SREBP2^{+} nuclei/total endothelial nuclei and found a significant increase in proliferating but not in involuting IH when compared to normal skin (Figure 4G). Moreover, we analyzed tissue from four patients with regrowing IH (n=4) (Figure 4D). These patients had received beta-blocker treatment during infancy with notable clinical response. However, the IH regrew significantly after discontinuation of treatment. All regrowing IH specimens were positive for nuclear SOX18 and SREBP2 along the endothelium at levels comparable to proliferating IH and significantly increased compared to the skin control (Figure 4A-D, G, Supplemental Figure 4.2). All tissue stainings were validated using primary and secondary antibody controls (Supplemental Figure 4.2-4).

We further tested if the SOX18-MVP axis is active in another pediatric vascular tumor – congenital hemangioma with its sub entities rapidly- and non-involuting congenital hemangioma (RICH and NICH)(28). We observed significantly increased $SOX18^{+}SREBP2^{+}$ endothelial cells in RICH and NICH compared to skin controls (Figure 4E, F; Supplemental Figure 4.2, Figure 4G). This adds new insights into these understudied pediatric vascular tumors. In summary, the differential nuclear co-localization of SOX18 and SREBP2 in different stages of IH underscores the role of the MVP in IH pathogenesis and may serve as a marker to predict therapy response. In addition, we quantified Ki67+ proliferating cells in IH, RICH and NICH and found significantly increased Ki67+ cells in RICH compared to normal skin controls, whereas proliferating, involuting, regrowing IH and NICH were not significantly increased (Supplemental Figure 4.1). Table 1 provides detailed patient information for samples used in Figure 4.

Statins inhibit vessel formation in a preclinical xenograft model of IH.

We surmised that if the MVP is critical to IH onset and progression, statins – competitive inhibitors of rate limiting enzyme in the MVP, HMGCR, – would inhibit HemSC blood vessel formation in a preclinical IH model. The effect of statins on HemSC cells has not been reported before and therefore we first tested for cell toxicity. We chose to use atorvastatin as it among the most commonly used statins in cardiovascular disease patients, and simvastatin due to pre-existing clinical trial data in infants with Smith-Lemli-Opitz syndrome (SLOS)(29). As atorvastatin is 5-10 times more potent than simvastatin, we adjusted the doses accordingly (30). To first address toxicity, HemSC (n=3 biological replicates) were treated with simvastatin (0.1 - 1 μM) or atorvastatin (0.01 - 0.1 μM). Neither statin affected HemSC viability at the given concentrations, compared to vehicle (DMSO) (Supplemental Figure 5.1).

Next, we tested 1 μM simvastatin and 0.1 μM atorvastatin on HemSC endothelial differentiation (12). Both statins significantly inhibited endothelial differentiation indicated by decreased expression of the EC markers CD31 and VE-Cadherin compared to vehicle control; R(+) propranolol was included as a positive control (Figure 5A). KLF2 and KLF4 were analyzed in the same HemSC to endothelial differentiation assay because of reported statin effects on these transcription factors (31, 32). Neither simvastatin, atorvastatin nor R(+) propranolol increased KLF2 and KLF4 in differentiating HemSC (Supplemental Figure 5.2).

We next tested if statins would impact de novo vessel formation in the murine xenograft model using IH-derived HemSC (n=4) (Figure 5B). Simvastatin at 10 mg/kg/day (Figure 5C,D) and atorvastatin at 1 mg/kg/d (Supplemental Figure 5.3) both significantly inhibited blood vessel formation seen by H&E

staining and by anti-human $CD31^+$ staining. A simvastatin dose response experiment showed 1 mg/kg/d was sufficient to significantly inhibit vessel formation (Figure 5E). Glucose levels and body weight of mice were unaffected (Figure 5F,G). The human equivalent doses corresponding to the doses used in mice are shown in Supplemental Figure 5, Table S5. The effective doses of simvastatin and atorvastatin in Figure 5 are below effective doses used in adults and significantly below the dose used in infants with SLOS (0.5 - 1 mg/kg/d simvastatin)(29, 33). Of note, the inhibitory effect of statins was limited to HemSC de novo vessel formation and did not impact angiogenic sprouting and ingrowth of surrounding murine vessels into the Matrigel implant (Supplemental Figure 5.4-5). In addition, Matrigel implant sections were stained and quantified for the proliferating cell maker Ki67. $Ki67^+$ cells were comparable in both groups, indicating proliferation *per se* was not affected by statins in this context (Figure 5H, I), consistent with the lack of effect of statins on HemSC and HemEC proliferation in vitro (Supplemental Figure 5.6). Taken together, this supports why we observed reduced redness but no decrease in size of Matrigel implants in the statin-treated xenograft mice - reflecting that differentiation rather than proliferation is the key event in IH vessel formation (Figure 5C). Specificity of the anti-human CD31 and anti-mouse CD31 antibodies was verified (Supplemental Figure 5.7). In summary, our data show that simvastatin and atorvastatin inhibit endothelial differentiation of HemSC in vitro and HemSC vasculogenesis in a preclinical IH xenograft model. This strongly suggests the MVP contributes to vasculogenesis in IH and can be effectively targeted by statins in a translational approach.

We next tested statin on HemSC microvascular mural cells (MMC) and adipogenic differentiation. MMC differentiation was induced by co-culture with HemEC for 5 days followed by immuno-separation with anti-CD31 (13, 34); immune separation was confirmed (Supplemental Figure 5.8). MMC genes *Calponin*, *PDGFRB*, *NG2*, and *TAGLN* were not affected by 0.1 uM atorvastatin or 0.5 uM simvastatin (Supplemental Figure 5.9). Similarly, atorvastatin or simvastatin treatment of HemSC undergoing adipogenic differentiation had no effect over 8 days of differentiation, quantified by Oil-Red-O staining (Supplemental Figure 5.10). Rapamycin served as a positive control for inhibition of HemSC adipogenic differentiation(35). Adipogenic genes *PPARg*, *cEBPa*, and *lipoprotein lipase* (*LPL*) were similarly unaffected by statin treatment (Supplemental Figure 5.11). In summary, this data suggests that statins inhibit endothelial differentiation of HemSC but not adipogenic or MMC differentiation.

Statin, R(+) propranolol, and rapamycin upregulation of the low-density lipoprotein receptor (LDL-R) in HemSC

A well-documented effect of statins is increased LDL-R expression. This is a compensatory response to offset the HMGCR inhibition to maintain cellular cholesterol levels(36, 37). Thus, we analyzed *LDL-R* expression in HemSC treated with R(+) propranolol or statins for 24 hours. Consistent with the R(+) propranolol inhibition of the MVP, R(+) propranolol significantly increased *LDL-R* expression to a similar extent as simvastatin and atorvastatin. We tested rapamycin as it has been used effectively for IH (38, 39) and because mTORC1 activates SREBP2(40); hence rapamycin may also impact the MVP in HemSC. Indeed, rapamycin significantly increased *LDL-R* levels. OX03050 - a squalene synthase 1 inhibitor - served as a positive control. Tipifarnib, a farnesyltransferase inhibitor acting downstream of the MVP, served as a negative control. Together, this provides another line of evidence for the response of HemSC to statins and shows similarly increased *LDL-R* by R(+) propranolol, statins, and rapamycin. This suggests combinations of these drugs targeting the SOX18-MVP axis at different levels might offer an innovative therapeutic approach to treat IH (Figure 6A). The schematic in Figure 6B illustrates points of inhibition for these drugs along the SOX18-MVP axis.

DISCUSSION:

In this study, we uncover an endothelial SOX18-MVP axis as a central regulator of IH pathogenesis. The R(+) enantiomer of propranolol, shown previously to disrupt SOX18 transcriptional activities, downregulates expression of MVP genes in a SOX18-dependent manner and it reduces mature SREBP2 protein, the master transcriptional regulator of the MVP. We propose that SOX18 augments the transcription of MVP genes to regulate cholesterol and isoprenoid biosynthesis in HemSC undergoing endothelial differentiation. Competitive inhibition of the rate-limiting enzyme of the MVP - HGMCR - with statins results in significantly reduced HemSC blood vessel formation in a preclinical IH xenograft model. Together, these results make a compelling case for the involvement of an endothelial SOX18-MVP axis in the etiology of IH and suggest statins may be a new therapeutic strategy. In line with our previously discovered drug mechanisms in IH - including corticosteroids, sirolimus, and propranolol (12, 13, 35, 41) - statins inhibit HemSC endothelial differentiation and have little effect on proliferation.

Additional experiments support these insights. R(+) propranolol or the SOX18 inhibitor Sm4 decreased new synthesis of cholesterol in HUVEC and the *RαOp* dominant negative SOX18 (42) downregulated HMGCS1 and HMGCR. Moreover, SOX18 ChIP binding sites are present in *HMGCS1* and *HMGCR*. We next found increased SOX18 and SREBP2 co-localized in endothelial nuclei in proliferating phase IH and four cases of regrowing IH, further connecting SOX18 to the MVP. Regrowing IH defies the classic IH life cycle, and little is known about how or why these IH regrow(43); most often, regrowing IH involves oral mucosa, such as the lip. Typically, propranolol therapy is restarted to prevent sequelae. In our four IH patients, regrowth occurred at 6-9 years of age. The nuclear co-localized SOX18 and SREBP2 in proliferating phase IH and regrowing IH suggests that $SOX18^{+}$/$SREBP2^{+}$ endothelial nuclei may serve as a biomarker for the vasculogenic capacity of the tumor.

SOX18 is a transcriptional regulator of vascular and lymphatic development, and tumor angiogenesis (16-18, 23, 44, 45). Notably, while glycolysis and fatty acid oxidation have been well established in physiological and pathological endothelial cell metabolism (46, 47), the MVP has not been implicated as a crucial regulatory pathway with the exception of one study in which single cell RNA sequencing of angiogenic endothelial cells identified *SQLE*, the gene that encodes squalene monooxygenase, as a metabolic angiogenic target (48). Our discovery of a functional link between the EC-specific SOX18 and the MVP brings to light what we consider an entirely novel concept in endothelial differentiation and vasculogenesis.

The MVP is central to cholesterol biosynthesis and isoprenoid biosynthesis, the latter needed for prenylation. The MVP bifurcates at farnesyl pyrophosphate (FPP) to produce squalene, an intermediate in cholesterol biosynthesis, or geranylgeranyl pyrophosphate (GGPP). FPP and GGPP are directly involved in prenylation of various small GTPases, and other protein substrates including RAS family members(49) . Importantly, RAS signaling has been implicated in IH (50). The R(+) propranolol mediated reduction in MVP genes and cholesterol biosynthesis may affect membrane fluidity and ruffling or activation of important signaling pathways via reduced prenylation. This warrants further investigation.

Pleiotropic benefits of statins, beyond lowering plasma LDL-cholesterol levels, are well documented. These include inhibiting inflammatory responses, increasing the bioavailability of nitric oxide, promoting re-reendothelialization, and reducing oxidative stress (51-53). The underlying mechanisms, however, remain elusive. A recent study suggests epigenetic effects: simvastatin significantly improved human induced pluripotent stem cell-derived endothelial cell function by reducing chromatin accessibility under physiological and pathological conditions (54). Interestingly, mTORC1 reduces ER cholesterol levels which in turn activates SREBP2 and the MVP (40), indicating rapamycin may indirectly inhibit the MVP.

Statins are widely used drugs. The resulting reduction in cholesterol synthesis increases LDL-receptor expression, which in turn clears LDL cholesterol from the circulation. In our study, statins, R(+) propranolol, and rapamycin significantly increased LDL receptor transcript levels in HemSC suggesting convergence of these drugs, each with distinct mechanism, on the MVP. This suggests a potential for combination therapy with potentially lower doses of each drug and fewer adverse effects. Statins are generally considered a safe and well tolerated drug class. They can be associated with an increased risk of muscle pain, diabetes mellitus and hepatic transaminase elevations, however, the risk of muscle symptoms from statin therapy is small and generally mild (55). We addressed potential side effects and did not observe a change in glucose levels or weight with simvastatin and atorvastatin in the xenografted mice over 7 days. A limitation is the relatively short treatment duration to detect adverse effects; moreover, adverse effects in rodents differ from those in humans. Bearing in mind drug safety as the highest priority when considering translating statins to infants, we performed a dose response experiment with simvastatin. The lowest dose that showed significant reduction in IH vessels in the xenograft model was 1 mg/kg/d (Figure 5E). This translates to a human equivalent dose of 0.081 mg/kg/d (56) (Supplemental Figure 5, Table 5.2), which is 6.25 times below the recommended dose of

0.5 mg/kg/d systemic simvastatin for infants with other indications. Further, topical rather than systemic statins might be used for superficial or less complex IH with increased safety as shown for other applications discussed below.

Systemic statins have been used safely in infants with Smith-Lemli-Opitz syndrome (SLOS), an autosomal-recessive syndrome characterized by the accumulation of 7-dehydrocholesterol. In a randomized, placebo-controlled clinical trial the recommended dose was 0.5 to 1 mg/kg/d (29, 33, 57, 58). Topical statins have been used for dermatological conditions such as the X-linked and dominant congenital hemidysplasia with ichthyosiform erythroderma and limb defects (CHILD) syndrome (59). In addition, statins have been applied to treat alopecia areata (60, 61). Based on the successful use of statins in children with these disorders, we suggest a safe repurposing of topical and/or systemic simvastatin to treat infants with IH.

It is exciting to speculate that the link between SOX18 and the MVP may have important implications for various pathophysiological conditions of the endothelium with disturbed vasculogenesis and angiogenesis, including developmental defects underlying vascular anomalies. Indeed, we found elevated $SOX18^{+}/SREBP2^{+}$ endothelial cells in the congenital hemangioma entities RICH and NICH suggesting further exploration of the MVP in other vascular anomalies is warranted.

In contrast to vascular malformations for which genetic drivers have been identified, the genetic basis of IH is unknown. The known driver mutations in vascular malformations have facilitated precision medicine by repurposing existing oncology drugs(62, 63). In contrast, critical molecular players in IH have been uncovered by studying mechanisms of action of serendipitously discovered drugs (12, 13, 35, 41). Herein, our discovery revealed a mechanistic link between the endothelial cell-specific transcription factor SOX18 and the MVP enabling molecularly characterized, targeted treatment approaches for IH.

The endothelial SOX18-MVP axis functionally connects the mechanisms of action of beta-blockers and statins. Of broader interest, beta-blocker or statin use in oncology patients in addition to standard treatment, has been shown to result in significantly improved cancer-related mortality in retrospective and prospective clinical trials in various entities (64-68). We speculate this may be due to the inhibition of the endothelial SOX18-MVP-axis in tumor endothelial cells.

In summary, our findings uncover an endothelial SOX18-MVP axis as a central molecular driver for IH vasculogenesis. Based on SOX18 loss and gain of function approaches, we surmise that SOX18 may act as an endothelial fine tuner for MVP activity. In a preclinical xenograft model with IH patient-derived cells, we show that simvastatin or atorvastatin inhibit IH vessel formation. This suggests statins could be repurposed to treat this common vascular tumor of infancy, topically or systemically.

METHODS:

Sex as a biological variable: Our study used male nude mice to xenograft hemangioma-derived cells isolated from male and female IH patients (see Table 1).

IH cell isolation and culture: The clinical diagnosis of IH was confirmed in the Department of Pathology of Boston Children's Hospital; IH specimens were de-identified as specified in Table 1. HemSC and HemEC were selected from IH single cell suspensions using anti-CD133- and anti-CD31-coated magnetic beads (Miltenyi Biotec), respectively, and expanded and cryopreserved. Cells were tested for mycoplasma by qPCR when cells were thawed and every 4-6 weeks thereafter. Cells were seeded on fibronectin-coated (0.1 μg/cm^2; MilliporeSigma) plates at 20,000 cells/cm^2 in Endothelial Growth Medium-2 (EGM-2; Lonza), which consists of Endothelial Basal Medium-2 (EBM-2; Lonza), SingleQuots (all except hydrocortisone and gentamicin-1000; Lonza), 10% heat-inactivated fetal bovine serum (FBS) (Cytiva), and 1× GPS (292 mg/mL glutamine, 100 U/mL penicillin, 100 mg/mL streptomycin; Mediatech). Hereafter, this full growth media is referred to as EGM-2. Cells were cultured at 37°C in a humidified incubator with 5% CO_2 and fed every other day.

Hemangioma endothelial differentiation assay: HemSC (samples denoted as HemSC 125, 149, 150, 165, 167, 171) were seeded on fibronectin-coated plates at a density of 20,000 cells/cm^2 in EGM-2. After 18 - 24 hours, cells were washed with EBM-2 once and starved for 16 hours in 2% BSA/serum-free EBM-2. Cells were washed again once with EBM-2 and induced to undergo EC differentiation in serum-free EBM-2 containing 1× insulin transferrin-selenium, 1:100 linoleic acid–albumin, 1 μM dexamethasone, and 100 μM ascorbic acid-2-phosphate±10 ng/mL VEGF-B (R&D Systems) on Day 0 and every two days thereafter. For addition of inhibitors, a preincubation ± respective inhibitors for 30 minutes was conducted followed by continuous treatment. Stock solutions of 10 mM R(+) propranolol hydrochloride (MilliporeSigma), 105 mM simvastatin, and 10 mM atorvastatin (both MilliporeSigma) were prepared in DMSO (MilliporeSigma). 20 μM R(+) propranolol was added for two hours and cells harvested for RNA sequencing (n=6) (Figure 1A,B,C). Continuous treatment with 1 μM simvastatin, 0.1 μM atorvastatin as well as 20 μM R(+) propranolol as a positive control was applied to differentiating HemSC (n=3) to test for an effect of statins in vitro (Figure 5A). Respective vehicle controls of each drug were used. Vehicle without VEGF-B served as a negative control and with VEGF-B as a positive control for differentiation.

Hemangioma microvascular mural cell (MMC) differentiation assay: HemSC denoted as *171* (Table 1) were seeded together with endothelial colony forming cells (ECFC) at a ratio of 1:1 at a total density of

30,000 cells/cm^2 on fibronectin-coated plates in EGM-2, as described(69). DMSO (MilliporeSigma) was added as a negative control, 25 µM DAPT (MilliporeSigma) was added as a positive control. After 4 hours, the culture media was changed to 0.5 µM simvastatin or 0.1 µM atorvastatin to determine effect on MMC differentiation. The media was changed every other day. Cells were cocultured for 5 days, harvested, and separated with immunomagnetic beads conjugated with anti-CD31 (Invitrogen) to obtain CD31+ (endothelial cells), and CD31- (HemSC and HemSC-derived MMC) (see schematic in Supplemental Figure 5.8).

Adipogenic differentiation assay: Racemic propranolol and R(+) propranolol (MilliporeSigma) were reconstituted at 10 mM in phosphate-buffered saline (PBS) for stock solution. Rapamycin (LC Laboratories) was reconstituted in DMSO to 10 mM for stock solution. On Day -1, HemSC were seeded at 20,000 cells/cm^2 in fibronectin-coated wells (0.1 µg/cm^2) on a 24-well plate and allowed to adhere overnight. Adipose mesenchymal stem cells (AMSC) served as controls. On Day 0, cells were washed with PBS and incubated in adipogenic media (AM), consisting of DMEM-high glucose (Gibco), 10% heat-inactivated FBS (Cytiva), 1x Penicillin-Streptomycin-L-Glutamine (GPS; Corning), 1µM dexamethasone (MilliporeSigma), 0.5mM 3-isobutyl-1-methylxanthine (MilliporeSigma), 5µg/ml insulin and 60 µM indomethacin (both MilliporeSigma). AM without dexamethasone, IBMX, insulin, and indomethacin served as the control and is denoted as *control media* in adipogenesis assays. The media was replaced every 48 hours. Adipogenic differentiation of HemSC was conducted over the course of 8 days, followed by Oil Red O staining and qPCR.

Cholesterol measurements in HUVEC: HUVEC were grown in EBM-2 media (Lonza, C2519A) supplemented with EGM-2 bullet kit (Lonza). HUVEC were seeded on 0.5% gelatin-coated 6-well plates at a density of 1.5 x10^5 cells/well overnight. The day after seeding cells were treated with 2.5mM MBCD (MilliporeSigma) to deplete cells of endogenous cholesterol. MBCD was withdrawn after 4 hours, cells were washed with PBS, and treated with either PBS, 20 µM R(+) propranolol (MilliporeSigma), DMSO, or 40 µM of Sm4 (MilliporeSigma) for 18 hours. Cells were then washed with PBS, trypsinized, washed with PBS, and centrifuged. Lipids were extracted from the cell pellets through one-phase extraction with 202 uL of BuOH:MeOH (1:1) (MilliporeSigma) that contains 10 µM of cholesterol-d7 (Cayman Chemical) as the internal standard (70). The cholesterol analysis was performed on a TSQ Altis triple quadrupole mass spectrometer, operated in positive ion mode, coupled to a Vanquish UHPLC system (Thermo Fisher) using the transition from precursor mass of *m/z* 369.3516 (MS1) to *m/z* 161.1 (MS3) for cholesterol and 376.4 to 161.1 for cholesterol-d7 (70). The solvent pair included solvent A (100% H2O, 0.1% FA and 2

mM NH_4COO^-) and solvent B (100% MeOH, 0.1% FA and 2 mM NH_4COO^-) with a flow rate at 0.3 mL/min (80% B at the start). Cholesterol and its deuterated standard were separated on an Eclipse Plus C8 column (Agilent), and peaks were integrated with TraceFinder 5.1 (Thermo Fisher) using the daughter ion at *m/z* 161.1 (Figure 2B,C) (71).

RaOp expression in HUVECs: HUVEC (Lonza, C2519A) were seeded and transfected the day after using X-tremeGene HP Transfection Reagent kit (Roche) to introduce 500ng of Halo-RaOp DNA using EBM-2 culture media without antibiotic. Cells were incubated at 37°C with 5% CO_2 overnight. The next day, cells were incubated with 5nM of JF646-Halo-ligand for 15min, washed with PBS and trypsinized; as a result, HUVEC expressing $SOX18^{RaOp}$ were fluorescently tagged. Cells were spun down, washed with PBS and permeabilized with 0.2% Triton X-100 for 10min, followed by blocking with 5% BSA/PBS for 1 hour. Cells were labelled with 1:300 dilution of anti-human HMGCR (Thermo Fisher, PA537367) or HMGCS1 (Thermo Fisher, PA513604) for 1 hour at room temperature in the dark. Cells were washed with PBS and stained with 1:500 dilution of anti-rabbit IgG conjugated with Alexa Fluor 488 (Invitrogen, A11008) for 30 min and washed with PBS. Cells were then imaged on a Fortessa X-20 (BD Bioscience). Data analysis was performed using FlowJo software.

Lentiviral overexpression and knockdown of SOX18: Undifferentiated HemSC were transduced with a lentivirus encoding SOX18 linked to GFP (custom lentivirus VB240403-1251jyg; Vector Builder) or an empty vector control virus (control lentivirus VB010000-9298rtf; Vector Builder). Successful lentiviral transduction was confirmed by nuclear GFP expression and overexpression efficiency was confirmed by WB (Supplemental Figure 3.3). Lentiviral knockdown of SOX18 in HemEC was performed with SOX18 shRNA lentivirus (TRCN0000017450; MilliporeSigma) or an empty vector control virus (SHC001V, MilliporeSigma) followed by puromycin (1 µg/mL) selection for 5 days. Thereafter, cells were maintained in EGM-2. Knockdown efficiency was confirmed by qPCR and WB. R(+) propranolol treatment of $HemSC^{SOX18OE}$ and $HemEC^{shSOX18}$ (samples denoted as $HemSC^{SOX18OE}$ 171 and $HemEC^{shSOX18}$ 133, 150 and 171), was for 24 hours.

Western Blot: HemSC were induced to undergo differentiation according to the protocol described above. Cells were treated with 20 µM R(+) propranolol for 2 hours on Day 6 of endothelial differentiation and lysed in a RIPA-based lysis buffer (25 mM Tris HCl pH 7.6, 150 mM NaCl, 1% NP-40, 1% sodium deoxycholate, 0.1% SDS) with protease and phosphatase inhibitors (Cell Signaling Technology) as well as calpain I and proteasome V inhibitors (MilliporeSigma). Cell extracts were electrophoresed by SDS-PAGE, transferred to nitrocellulose or to PDVF and probed with anti-SREBP2

clone 22D5(72) (1:200, MilliporeSigma, MABS1988) followed by anti-GAPDH (1:2000, Cell Signaling Technology, 5014). For protein quantification of SOX18 overexpression efficiency in HemSC^{SOX18OE} and knockdown efficiency in HemEC^{shSOX18}, cells were seeded on fibronectin-coated plates (0.1 µg fibronectin/cm^2) at a density of 20,000 cells/cm^2 in EGM-2 media, lysed and processed as described above following staining with SOX18 (D-8) (1:500, Santa Cruz Biotechnology, sc-166025) and GAPDH (Cell Signaling Technology) antibodies. All signals were detected by ECL. The densitometric analysis was conducted using Fiji ImageJ software.

In vivo murine model for human blood vessel formation: Experiments were carried out with 3×10^6 HemSC per implant. HemSC (n=4, samples 125, 147, 149, 150) were grown in EGM-2 media until 90% confluent. A stock solution of simvastatin (105 mM; MilliporeSigma) or atorvastatin (10 mM; MilliporeSigma) was prepared in DMSO. Twenty-four hours before trypsin removal from plates, 1 µM simvastatin or 0.1 µM atorvastatin or the equivalent DMSO concentration as a control was added to the media. Cells were counted after the 24-hour pretreatment and suspended in 200 µL Matrigel (Corning) including 1 µg/mL basic FGF (ProSpec), 1 µg/mL erythropoietin (ProSpec), and 0.5 µM (simvastatin) or 0.05 µM (atorvastatin) or vehicle (DMSO) on ice. The Matrigel/cell suspensions were injected subcutaneously into the flanks of 6-7-week-old male athymic nude mice, strain Hsd: Athymic Nude-Foxn1nu (Envigo, 6904M), placing 2 implants per mouse (n = 3-5 mice/group; Figure 5B). The mice were treated with 0.1 - 50 mg/kg/d simvastatin, 1 - 15 mg/kd/d atorvastatin or the equivalent DMSO concentration as a control (200 µL/mouse, i.p.) every 12 hours. Blood glucose levels were measured daily before the morning i.p. injection. Glucose concentrations were measured in tail vein blood using the OneTouch UltraSmart Blood Glucose Monitoring System (LifeScan). Body weight was measured before the injections (day 0), on day 4 and before removal of the implants (day 8). After 8 days, the mice were euthanized and the implants were removed, photographed, fixed in formalin, embedded in paraffin, and analyzed by H&E staining and immunofluorescent staining (IF). Blood vessels (indicated by luminal structures containing one or more RBCs) and CD31$^+$ stained human vessels were counted in 5 fields/section, 2 sections/implant. Each field was 425.1 µm × 425.1 µm = 0.18071 mm2, and sections were from the middle of the implant. Vessel density is expressed as vessels/mm^2.

H&E and immunofluorescent staining of Matrigel implant and human FFPE tissue sections: FFPE tissue sections (5 µm) of the Matrigel implants were deparaffinized and either directly stained with H&E or immersed in an antigen retrieval solution (citrate-EDTA buffer containing 10 mM citric acid, 2 mM EDTA, and 0.05% Tween-20, pH 6.2) for 20 minutes at 95°C–99°C. Sections were subsequently blocked for 30

minutes in TNB Blocking Buffer (PerkinElmer) followed by incubation with a mouse anti-human CD31 monoclonal antibody (1:30; Dako, Glostrup, 0823) to stain for human endothelium. Next, sections were incubated with Alexa Fluor 647 chicken anti-mouse IgG (1:200, Invitrogen, A-21463) as a secondary antibody. An anti-mouse-specific CD31 monoclonal antibody (1:100, R&D Systems, AF3628) was used to quantify mouse vessels in the Matrigel implants. Alexa Fluor 647 chicken anti-goat IgG was applied as a secondary antibody (1:200, Invitrogen, A-21469). Tissue specificity of the anti-human and anti-mouse antibodies was confirmed by negative staining in mouse lung and human skin tissue, respectively (see Supplemental Figure 5.7). FFPE tissue sections (5 µm) from patients with IH or with congenital hemangioma were deparaffinized, immersed in an antigen retrieval solution, and blocked for 30 min in 10% donkey serum followed by incubation with mouse anti-human SOX18 (D-8) (1:50, Santa Cruz Biotechnology, sc-166025), rabbit anti-human SREBP2 (1:100, Abcam, ab30682), or rabbit- anti human Ki67 (1:100, Abcam, ab15580) and UEA1 fluorescently labeled with Alexa Fluor 649 (1:50, Vector Laboratories, DL1068). Next, the sections were incubated with Alexa Fluor 488 donkey anti-mouse IgG (1:200; Invitrogen, A-21202) and Alexa Fluor 546 donkey anti-rabbit IgG (1:200; Invitrogen, A-10040) as secondary antibodies. All slides were mounted using DAPI (Molecular Probes) to visualize nuclei. IF Images were acquired by a LSM 880 confocal microscope (Zeiss). Images were analyzed through a 20x or 63x objective lens. All images were analyzed using Fiji ImageJ software.

Oil Red O-staining: The Oil Red O working solution (ORO; MilliporeSigma) was freshly prepared in a 3:2 ratio of 0.5% (w/v) ORO in isopropanol (Fisher Scientific) and double distilled H2O (ddH2O) and was filtered to remove precipitates. For ORO staining of lipid droplets, 12 mm coverslips (Electron Microscopy Sciences) were coated with fibronectin (0.1 µg/cm^2) in 24-well plates before seeding of HemSC. Cells were fixed in 4% paraformaldehyde (Electron Microscopy Sciences) for 15 minutes at room temperature, washed in PBS, and incubated in 60% isopropanol for 3 minutes. Cells were stained with ORO for 10 minutes at room temperature and washed with 60% isopropanol for 10 minutes to remove unbound ORO dye. Cells were washed in ddH2O, mounted onto slides, and imaged within 24-48 hours to avoid precipitation.

Immunofluorescent cell staining: $HemEC^{Ctr}$ and $HemEC^{shSOX18}$ were seeded on fibronectin-coated plates at a density of 30,000 cells/cm^2 in EGM-2 media for 30 hours on 2 cm^2 slides, fixed in 4% PFA and blocked in 5% BSA/0.3% Triton x-100 for 1 hour. The mouse anti-human SOX18 used for immunostaining (D-8) was validated in $HemEC^{Ctr}$ and $HemEC^{shSOX18}$ (1:100 Santa Cruz Biotechnology, sc-166025) Figure 3L,M). Cells were co-stained with a rabbit anti-human SREBP2 (1:200, Abcam, ab30682). Secondary

antibodies included Alexa Fluor 488 donkey anti-mouse IgG (1:200; Invitrogen, A-21202) and Alexa Fluor 546 donkey anti-rabbit IgG (1:200; Invitrogen, A-10040). DAPI was used to visualize nuclei (Molecular probes followed by mounting (Invitrogen). Immunostainings of IH sections with respective isotype matched control IgG and secondary antibodies were conducted.

RNA isolation and qPCR: Total RNA was extracted from cells with the RNeasy Micro Extraction Kit (QIAGEN). Reverse transcriptase reactions were performed using an iScript cDNA Synthesis Kit (Bio-Rad). qPCR was performed using SYBR FAST ABI Prism 2× qPCR Master Mix (Kapa BioSystems). Amplification was carried out in a QuantStudio 6 Flex Real-Time PCR System (Fisher Scientific). A relative standard curve for each gene amplification was generated to determine the amplification efficiency, with greater than 90% considered acceptable. Fold increases in gene expression were calculated according to the ΔΔCt method, with each amplification reaction performed in duplicate or triplicate (73). Gene expression was normalized to the PBS or DMSO treatment, respectively. ATP5B was used as housekeeping gene expression reference. A list of all primer sequences used in this study is attached below.

Gene	Forward	Reverse
ATP5B	CCACTACCAAGAAGGGATCTATCA	GGGCAGGGTCAGTCAAGTC
Calponin	CCCAGAAGTATGACCACCAG	GCAGCTTATTGATGAATTCGC
CD31	CACCTGGCCCAGGAGTTTC	AGTACACAGCCTTGTTGCCATGT
cEBPa	TGGACAAGAACAGCAACGAG	TTGTCACTGGTCAGCTCCAG
HMGCR	AGTGAGATCTGGAGGATCCAA	GATGGGAGGCCACAAAGAGG
HMGCS1	ACACAAGATGCTACACCGGG	TGGGTGTCCTCTCTGAGCTT
KLF2	CTACACCAAGAGTTCGCATCTG	CCGTGTGCTTTCGGTAGTG
KLF4	CGAACCCACACAGGTGAGAA	TACGGTAGTGCCTGGTCAGTTC
LDL-R	CTACAGCTACCCCTCCAGAC	GGGACTCCAGGCAGATGTTC
LPL	GTCAGAGCCAAAAGAAGCAGC	ATGGGTTTCACTCTCAGTCCC
MVK	AGATCCCAAACCCGCTGAAG	CCTTGATGGTATCGGAGGGC
NG2	CCTGGAGAATGGTGGAAGAG	CTGTGTTTGTAGTGAGGATGG
NOTCH1	CGGTGAGACCTGCCTGAATG	GCATTGTCCAGGGGTGTCAG
PDGFRB	CGGAAATAACTGAGATCACCA	TTGATGGATGACACCTGGAG
PPARg	GCTGGCCTCCTTGATGAATA	TTGGGCTCCATAAAGTCACC
S1P	AGTTGGGAGTAAACAGCCCC	TCAATCAACCACTGTGAGCC
S2P	ACGGCGGAAAGCAAGGATGCTT	GTGCCAAAGTCTGCATCAGCGT
SCAP	GTGGACTCTGACCGCAAACAA	CGGGACAAAGGTGAACGAAATAC
SOX18	CAAGATGCTGGGCAAAGCGTG	GCGGGGGCGCTAATCC
SREBP2	ACAAGTCTGGCGTTCTGAGG	ACCAGACTGCCTAGGTCGAT
TAGLN	GAGGAATTGATGGAAACCACCG	CTCATGCCATAGGAAGGACCC
VE-Cadherin	CCTTGGGTCCTGAAGTGACCT	AGGGCCTTGCCTTCTGCAA

593 *Proliferation assay:* Cells were plated on 96-well plates with 1500 cells per well and cultured in EGM-2

for 4 hours. The medium was removed and replaced with 0.1 mL of fresh EGM-2 containing R(+) propranolol, simvastatin, atorvastatin, OXO3050 or rapamycin (all MiliporeSigma). The plates were incubated for 24 and 48 hours. After the treatment, 20 µL of MTS (CellTiter 96 AQueous One Solution Cell Proliferation Assay, Fisher Scientific) labeling reagent was added to each well, and plates incubated for another 2 hours. The spectrophotometric absorbance of the samples was detected by using a FilterMax F3 microplate reader (Molecular Devices) at 492 nm.

Bioinformatic analysis:

Bulk RNA-seq: We used trimmomatic v0.39 (74) to trim the low-quality next generation sequencing (NGS) reads (-threads 20 ILLUMINACLIP:TruSeq3-PE.fa:2:30:10 LEADING:3 TRAILING:3 SLIDINGWINDOW:4:15 MINLEN:36). Subsequently, only the high-quality trimmed reads were aligned to the human reference genome (hg38) using STAR v2.7.2b . The reads counts were calculated by featureCounts software (75). Differentially expressed genes (DEGs) were identified by using the DESeq2 R package (adjusted p-value < 0.05). KEGG pathways and gene ontology (GO) enrichment tests were performed by the clusterProfiler R package. A pathway or GO term was treated as significantly enriched if an adjusted p-values (with Benjamini-Hochberg correction) was smaller than 0.05. The bar plots illustrating significant pathway or GO terms were created using the enrichplot R package.

ChIP-seq: The data is displayed on the UCSC genome browser. The layered epigenetic marks dataset is supplied from Encode. The ChIP-seq binding location dataset can be found at https://www.ebi.ac.uk/biostudies/arrayexpress/studies/E-MTAB-4481.

Data collection and statistics: Data were analyzed and plotted using GraphPad Prism 10.1.0 (GraphPad Software). Results are displayed as the mean ± SD. For experiments in which cells were treated with drugs, the differences were assessed by one-way ANOVA. Tukey's post hoc test was used for multiple comparisons of different treatment modalities and Šidák's, Tukey's or Dunnett's test for multiple comparisons to compare every treatment mean with that of the respective vehicle control. A two-tailed, unpaired t-test was applied for comparisons between treatment and control groups given equal variance. Differences were considered significant for *P* values less than 0.05. Figures were created using Illustrator; schematics were in part created using Biorender.

Study approval: Animal protocols complied with NIH Animal Research Advisory Committee guidelines and were approved by the Boston Children's Hospital IACUC (protocol number 00001741). IH specimens were obtained under a protocol approved by Boston Children's Hospital (IRB protocol number 04-12-

175R; AH, HK, JBM, JB) as well as at Stanford University (IRB protocol number 35473; RL, JT). Hemangioma specimens were collected upon written informed consent of the patient's guardian, deidentified, and used for cell isolation under IRB approved protocol 04-12-175R and in accordance with Declaration of Helsinki principles.

Data availability: The bulk RNA-seq data can be accessed at the Gene Expression Omnibus archive at the National Center for Biotechnology Information under accession number GSE274946 (Day 6) and GSE275019 (Day 4). The supporting data values are are compiled in an XLS file.

Acknowledgements

We thank the Vascular Anomalies Center and Department of Pathology at Boston Children's Hospital for patient specimens. We thank Dr. Andreane Cartier and Dr. Sandra Schrenk for technical advice and Trisha Lopez for patient chart reviews. Research reported in this manuscript was supported by NIH grant 5R01HL096384 (to JB). AH was supported by DFG, German Research Foundation (grant 458322953) and the Vascular Anomalies Center at Boston Children's Hospital. MF, MG were supported by the National Health and Medical Research Council, GNT1164000 and 5R01HL096384. AH and MV are members of the Vascular Anomalies Working Group (VASCA) of the European Reference Network for Rare Multisystemic Vascular Diseases (VASCERN) - Project ID: 769036. The funders had no role in the study design, data collection and interpretation, or decision to submit this work for publication.

Author contributions

AH, MG, MF, and JB designed the study. AH, MG, JWS, JWHT, MAH, LB, and LC conducted experiments. AH, MG, JWS, JWHT, MAH, LB, LC, AJ, and MS carried out formal analysis. RL, HK, JCT, and JBM provided patient specimens and clinical expertise. AH performed patient data curation. AH and JB wrote the original manuscript. All authors reviewed, edited, and agreed to the final version of the manuscript. AH, MV, MF, and JB acquired funding.

Conflict-of-interest statement

MF is involved with the startup biotech company GBM Pty Ltd., which develops SOX18 small-molecule inhibitors. All other authors declare no competing interests.

Intellectual property

AH and JB are co-inventors on a filed US patent application PCT/US23/83306 "Methods and Compositions for the Treatment of Vascular Anomalies." JB is co-inventor on US Patent #9,737,514.

REFERENCES:

1. Mulliken JB, and Glowacki J. Hemangiomas and vascular malformations in infants and children: a classification based on endothelial characteristics. *Plast Reconstr Surg.* 1982;69(3):412-22.
2. Khan ZA, et al. Multipotential stem cells recapitulate human infantile hemangioma in immunodeficient mice. *Journal of Clinical Investigation.* 2008;118(7):2592-9.
3. Xiang S, et al. Insights into the mechanisms of angiogenesis in infantile hemangioma. *Biomed Pharmacother.* 2024;178:117181.
4. Holm A, Mulliken JB, and Bischoff J. Infantile hemangioma: the common and enigmatic vascular tumor. *J Clin Invest.* 2024;134(8).
5. Leaute-Labreze C, Harper JI, and Hoeger PH. Infantile haemangioma. *Lancet.* 2017;390(10089):85-94.
6. Leaute-Labreze C, et al. A randomized, controlled trial of oral propranolol in infantile hemangioma. *N Engl J Med.* 2015;372(8):735-46.
7. Leaute-Labreze C, et al. Safety of Oral Propranolol for the Treatment of Infantile Hemangioma: A Systematic Review. *Pediatrics.* 2016;138(4).
8. Pope E. Commentary:Beta-blockers and sleep problems. *Pediatr Dermatol.* 2021;38(2):378-9.
9. Hermans MM, et al. Long-term neurocognitive functioning of children treated with propranolol or atenolol for infantile hemangioma. *Eur J Pediatr.* 2023;182(2):757-67.
10. Opri F, et al. Assessing Response Rates and Sleep Disorder Prevalence: Insights from a Propranolol Treatment Study for Infantile Haemangiomas. *Children (Basel).* 2024;11(9).
11. Mehvar R, and Brocks DR. Stereospecific pharmacokinetics and pharmacodynamics of beta-adrenergic blockers in humans. *J Pharm Pharm Sci.* 2001;4(2):185-200.
12. Overman J, et al. R-propranolol is a small molecule inhibitor of the SOX18 transcription factor in a rare vascular syndrome and hemangioma. *Elife.* 2019;8.
13. Seebauer CT, et al. Non-beta blocker enantiomers of propranolol and atenolol inhibit vasculogenesis in infantile hemangioma. *J Clin Invest.* 2022;132(3).
14. Fontaine F, et al. Small-Molecule Inhibitors of the SOX18 Transcription Factor. *Cell Chem Biol.* 2017;24(3):346-59.
15. Irrthum A, et al. Mutations in the transcription factor gene SOX18 underlie recessive and dominant forms of hypotrichosis-lymphedema-telangiectasia. *Am J Hum Genet.* 2003;72(6):1470-8.
16. Patel J, et al. Functional Definition of Progenitors Versus Mature Endothelial Cells Reveals Key SoxF-Dependent Differentiation Process. *Circulation.* 2017;135(8):786-805.
17. Francois M, et al. Sox18 induces development of the lymphatic vasculature in mice. *Nature.* 2008;456(7222):643-7.
18. Young N, et al. Effect of disrupted SOX18 transcription factor function on tumor growth, vascularization, and endothelial development. *J Natl Cancer Inst.* 2006;98(15):1060-7.
19. Zhang C, et al. Key Enzymes for the Mevalonate Pathway in the Cardiovascular System. *J Cardiovasc Pharmacol.* 2021;77(2):142-52.
20. Horton JD, Goldstein JL, and Brown MS. SREBPs: activators of the complete program of cholesterol and fatty acid synthesis in the liver. *J Clin Invest.* 2002;109(9):1125-31.

21. Chou R, et al. Statins for Prevention of Cardiovascular Disease in Adults: Evidence Report and Systematic Review for the US Preventive Services Task Force. *JAMA.* 2016;316(19):2008-24.
22. Schmitz G, and Langmann T. Structure, function and regulation of the ABC1 gene product. *Curr Opin Lipidol.* 2001;12(2):129-40.
23. Overman J, et al. Pharmacological targeting of the transcription factor SOX18 delays breast cancer in mice. *Elife.* 2017;6.
24. Pennisi D, et al. Mutations in Sox18 underlie cardiovascular and hair follicle defects in ragged mice. *Nat Genet.* 2000;24(4):434-7.
25. Radhakrishnan A, et al. Switch-like control of SREBP-2 transport triggered by small changes in ER cholesterol: a delicate balance. *Cell Metab.* 2008;8(6):512-21.
26. Chen L, et al. Endogenous sterol intermediates of the mevalonate pathway regulate HMGCR degradation and SREBP-2 processing. *J Lipid Res.* 2019;60(10):1765-75.
27. Downes M, and Koopman P. SOX18 and the transcriptional regulation of blood vessel development. *Trends Cardiovasc Med.* 2001;11(8):318-24.
28. Olsen GM, Nackers A, and Drolet BA. Infantile and congenital hemangiomas. *Semin Pediatr Surg.* 2020;29(5):150969.
29. Wassif CA, et al. A placebo-controlled trial of simvastatin therapy in Smith-Lemli-Opitz syndrome. *Genet Med.* 2017;19(3):297-305.
30. Jones P, et al. Comparative dose efficacy study of atorvastatin versus simvastatin, pravastatin, lovastatin, and fluvastatin in patients with hypercholesterolemia (the CURVES study). *Am J Cardiol.* 1998;81(5):582-7.
31. Parmar KM, et al. Statins exert endothelial atheroprotective effects via the KLF2 transcription factor. *J Biol Chem.* 2005;280(29):26714-9.
32. Yoshida T, et al. Endothelial Kruppel-Like Factor 4 Mediates the Protective Effect of Statins against Ischemic AKI. *J Am Soc Nephrol.* 2016;27(5):1379-88.
33. Jira PE, et al. Simvastatin. A new therapeutic approach for Smith-Lemli-Opitz syndrome. *J Lipid Res.* 2000;41(8):1339-46.
34. Boscolo E, Mulliken JB, and Bischoff J. VEGFR-1 mediates endothelial differentiation and formation of blood vessels in a murine model of infantile hemangioma. *Am J Pathol.* 2011;179(5):2266-77.
35. Greenberger S, et al. Rapamycin suppresses self-renewal and vasculogenic potential of stem cells isolated from infantile hemangioma. *J Invest Dermatol.* 2011;131(12):2467-76.
36. Goldstein JL, and Brown MS. The LDL receptor. *Arterioscler Thromb Vasc Biol.* 2009;29(4):431-8.
37. Goldstein JL, and Brown MS. A century of cholesterol and coronaries: from plaques to genes to statins. *Cell.* 2015;161(1):161-72.
38. Davila-Osorio VL, et al. Propranolol-resistant infantile hemangioma successfully treated with sirolimus. *Pediatr Dermatol.* 2020;37(4):684-6.
39. Kleinman EP, et al. Sirolimus for diffuse intestinal infantile hemangioma with PHACE features: systematic review. *Pediatr Res.* 2023;93(6):1470-9.
40. Eid W, et al. mTORC1 activates SREBP-2 by suppressing cholesterol trafficking to lysosomes in mammalian cells. *Proc Natl Acad Sci U S A.* 2017;114(30):7999-8004.

41. Greenberger S, et al. Corticosteroid suppression of VEGF-A in infantile hemangioma-derived stem cells. *N Engl J Med.* 2010;362(11):1005-13.
42. McCann AJ, et al. A dominant-negative SOX18 mutant disrupts multiple regulatory layers essential to transcription factor activity. *Nucleic Acids Res.* 2021;49(19):10931-55.
43. Shah SD, et al. Rebound Growth of Infantile Hemangiomas After Propranolol Therapy. *Pediatrics.* 2016;137(4).
44. Herpers R, et al. Redundant roles for sox7 and sox18 in arteriovenous specification in zebrafish. *Circ Res.* 2008;102(1):12-5.
45. Donovan P, et al. Endovascular progenitors infiltrate melanomas and differentiate towards a variety of vascular beds promoting tumor metastasis. *Nat Commun.* 2019;10(1):18.
46. Eelen G, et al. Endothelial Cell Metabolism. *Physiol Rev.* 2018;98(1):3-58.
47. Zeng Q, et al. Understanding tumour endothelial cell heterogeneity and function from single-cell omics. *Nat Rev Cancer.* 2023;23(8):544-64.
48. Rohlenova K, et al. Single-Cell RNA Sequencing Maps Endothelial Metabolic Plasticity in Pathological Angiogenesis. *Cell Metab.* 2020;31(4):862-77 e14.
49. Tate EW, et al. Protein lipidation in cancer: mechanisms, dysregulation and emerging drug targets. *Nat Rev Cancer.* 2024;24(4):240-60.
50. Hu W, et al. NOGOB receptor-mediated RAS signaling pathway is a target for suppressing proliferating hemangioma. *JCI Insight.* 2021;6(3).
51. Laufs U, et al. Upregulation of endothelial nitric oxide synthase by HMG CoA reductase inhibitors. *Circulation.* 1998;97(12):1129-35.
52. Wolfrum S, Jensen KS, and Liao JK. Endothelium-dependent effects of statins. *Arterioscler Thromb Vasc Biol.* 2003;23(5):729-36.
53. Sen-Banerjee S, et al. Kruppel-like factor 2 as a novel mediator of statin effects in endothelial cells. *Circulation.* 2005;112(5):720-6.
54. Liu C, et al. Statins improve endothelial function via suppression of epigenetic-driven EndMT. *Nat Cardiovasc Res.* 2023;2(5):467-85.
55. Cholesterol Treatment Trialists C. Effect of statin therapy on muscle symptoms: an individual participant data meta-analysis of large-scale, randomised, double-blind trials. *Lancet.* 2022;400(10355):832-45.
56. Nair AB, and Jacob S. A simple practice guide for dose conversion between animals and human. *J Basic Clin Pharm.* 2016;7(2):27-31.
57. Chan YM, et al. Effects of dietary cholesterol and simvastatin on cholesterol synthesis in Smith-Lemli-Opitz syndrome. *Pediatr Res.* 2009;65(6):681-5.
58. Svoboda MD, et al. Treatment of Smith-Lemli-Opitz syndrome and other sterol disorders. *Am J Med Genet C Semin Med Genet.* 2012;160C(4):285-94.
59. Christiansen AG, Koppelhus U, and Sommerlund M. Skin Abnormalities in CHILD Syndrome Successfully Treated with Pathogenesis-based Therapy. *Acta Derm Venereol.* 2015;95(6):752-3.
60. Cervantes J, et al.Treatment of Alopecia Areata with Simvastatin/Ezetimibe. *J Investig Dermatol Symp Proc.* 2018;19(1):S25-S31.
61. Shin JM, et al. Putative therapeutic mechanisms of simvastatin in the treatment of alopecia areata. *J Am Acad Dermatol.* 2021;84(3):782-4.

62. Queisser A, et al. Genetic Basis and Therapies for Vascular Anomalies. *Circ Res.* 2021;129(1):155-73.
63. Dompmartin A, et al. The VASCERN-VASCA Working Group Diagnostic and Management Pathways for Venous Malformations. *J Vasc Anom (Phila).* 2023;4(2):e064.
64. Hiller JG, et al. Preoperative beta-Blockade with Propranolol Reduces Biomarkers of Metastasis in Breast Cancer: A Phase II Randomized Trial. *Clin Cancer Res.* 2020;26(8):1803-11.
65. Albinana V, et al. Propranolol: A "Pick and Roll" Team Player in Benign Tumors and Cancer Therapies. *J Clin Med.* 2022;11(15).
66. Poynter JN, et al. Statins and the risk of colorectal cancer. *N Engl J Med.* 2005;352(21):2184-92.
67. Nielsen SF, Nordestgaard BG, and Bojesen SE. Statin use and reduced cancer-related mortality. *N Engl J Med.* 2012;367(19):1792-802.
68. Scott OW, et al. Post-diagnostic statin use and breast cancer-specific mortality: a population-based cohort study. *Breast Cancer Res Treat.* 2023;199(1):195-206.
69. Boscolo E, et al. JAGGED1 signaling regulates hemangioma stem cell-to-pericyte/vascular smooth muscle cell differentiation. *Arteriosclerosis, thrombosis, and vascular biology.* 2011;31(10):2181-92.
70. Huynh K, et al. High-Throughput Plasma Lipidomics: Detailed Mapping of the Associations with Cardiometabolic Risk Factors. *Cell Chemical Biology.* 2019;26(1):71-84.e4.
71. Liu XT, et al. Ablation of sphingosine kinase 2 suppresses fatty liver-associated hepatocellular carcinoma via downregulation of ceramide transfer protein. *Oncogenesis.* 2022;11(1).
72. McFarlane MR, et al. Scap is required for sterol synthesis and crypt growth in intestinal mucosa. *J Lipid Res.* 2015;56(8):1560-71.
73. Schmittgen TD, and Livak KJ. Analyzing real-time PCR data by the comparative C(T) method. *Nat Protoc.* 2008;3(6):1101-8.
74. Bolger AM, Lohse M, and Usadel B. Trimmomatic: a flexible trimmer for Illumina sequence data. *Bioinformatics.* 2014;30(15):2114-20.
75. Liao Y, Smyth GK, and Shi W. featureCounts: an efficient general purpose program for assigning sequence reads to genomic features. *Bioinformatics.* 2014;30(7):923-30.

Sample ID	Sex	Location	Age at resection	Figure
				820
Proliferating IH (<1 year of age)				
P-150	M	R occiput	3m	1, 2, 3, 4, 5
P-147	M	R upper eyelid	3m	4, 5
P-138	F	L ear	3m	4
P-133	M	Upper forehead	3m	2, 3, 4
P-171	F	R brow	4m	1, 2, 3, 4, 5, 6
P-165	F	Lower occipital scalp	4m	1, 4, 6
P-168	F	L posterior scalp	5m	4
P-125	F	L abdominal wall	5m	1, 5
P-167	F	R abdominal wall	7m	1, 4
P-149	F	R scapula	7m	1, 4, 5
Involuting IH (>1 year of age)				
I-69	F	R calf	1y 1m	4
I-79	F	Nasal tip	1y 6m	4
I-71	F	R labium majus	2y 1m	4
I-85	M	L chin	2y 2m	4
I-99	M	L forehead	2y 6m	4
I-84	M	Nasal tip	2y 6m	4
I-78	M	Nasal tip	2y 6m	4
I-67	M	R cheek	2y 6m	4
I-81	F	R temporal area	2y 11m	4
I-68	F	R frontoparietal scalp	2y 11m	4
Regrowing IH				
R-1	F	R segmental distribution along V3	6y 4m	4
R-2	F	Lower lip	9y 6m	4
R-3	F	Lower lip	5y 8m	4
R-4	F	Lower lip, R temporal area	10y 6m	4
Rapidly involuting and non-involuting congenital hemangioma (RICH and NICH)				
RICH-1	M	R forearm	2y 9m	4
RICH-2	M	R mastoid scalp	6 m	4
RICH-3	F	R upper arm	1y 3m	4
NICH-1	M	L chest	7y 7m	4
NICH-2	M	L trunk	8y 6m	4
NICH-3	M	Perineum	12y 3m	4
Skin Controls				
C-1	M	Foreskin	8m	4
C-2	M	Foreskin	1y	4
C-3	F	Nevus	7y	4
C-4	M	Breast	17y	4

F: Female; L: Left; M: Male; m: month(s); R: Right; y: years; V3: third branch of trigeminal nerve

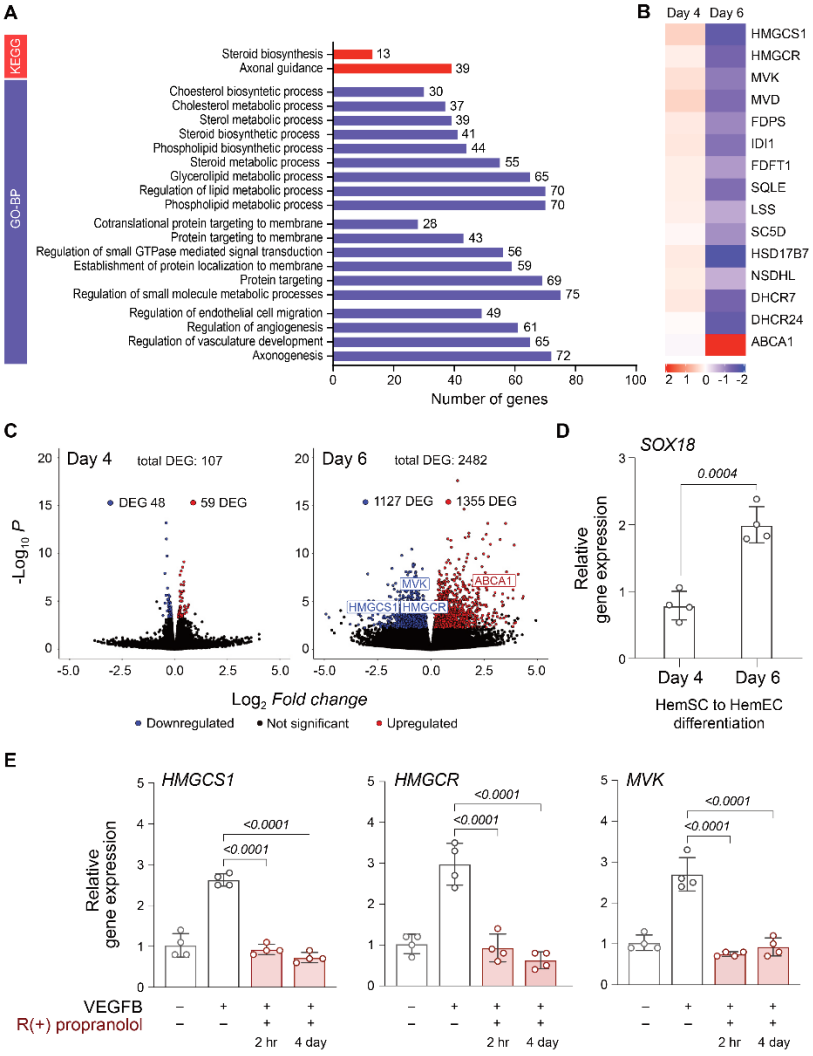

Figure 1. R(+) propranolol reduces MVP transcripts in IH -derived HemSC undergoing endothelial differentiation. HemSC in panels (**A**-**C**) were treated ± R(+) propranolol for 2 hours prior to RNA isolation. (**A**) *KEGG* pathway analysis and gene ontology analysis GO-BP of bulk RNA-seq data from HemSC treated on Day 6 of endothelial differentiation (n=6 biological replicates) ± R(+) propranolol showing the number of differentially expressed genes (DEGs), defined as Log_2 fold change >1 and adjusted p-value <0.05). (**B**) Heat map of differentially expressed MVP genes at Day 4 and Day 6. (**C**) Volcano plots of DEGs on Day 4 and Day 6 of HemSC to HemEC differentiation ($-Log_{10}$ for adjusted p value). (**D**) SOX18 mRNA levels on Day 4 and Day 6 (n=3 biological replicates; 1 of the biological replicates analyzed in two independent experiments yielding n=4 data points). (**E**) HemSC induced to undergo endothelial differentiation were treated ± R(+) propranolol for 2 hours on Day 6 or treated continuously from Day 2-6. qPCR analyses for *HMGCS1*, *HMGCR*, and *MVK* (n=3 biological replicates; 1 of the biological replicates analyzed in two independent experiments yielding n=4 data points). P values calculated using a two-tailed, unpaired t-test (**D**) and by a one-way ANOVA multiple comparisons test with Šidák-correction (**E**). Data show the mean ± SD.

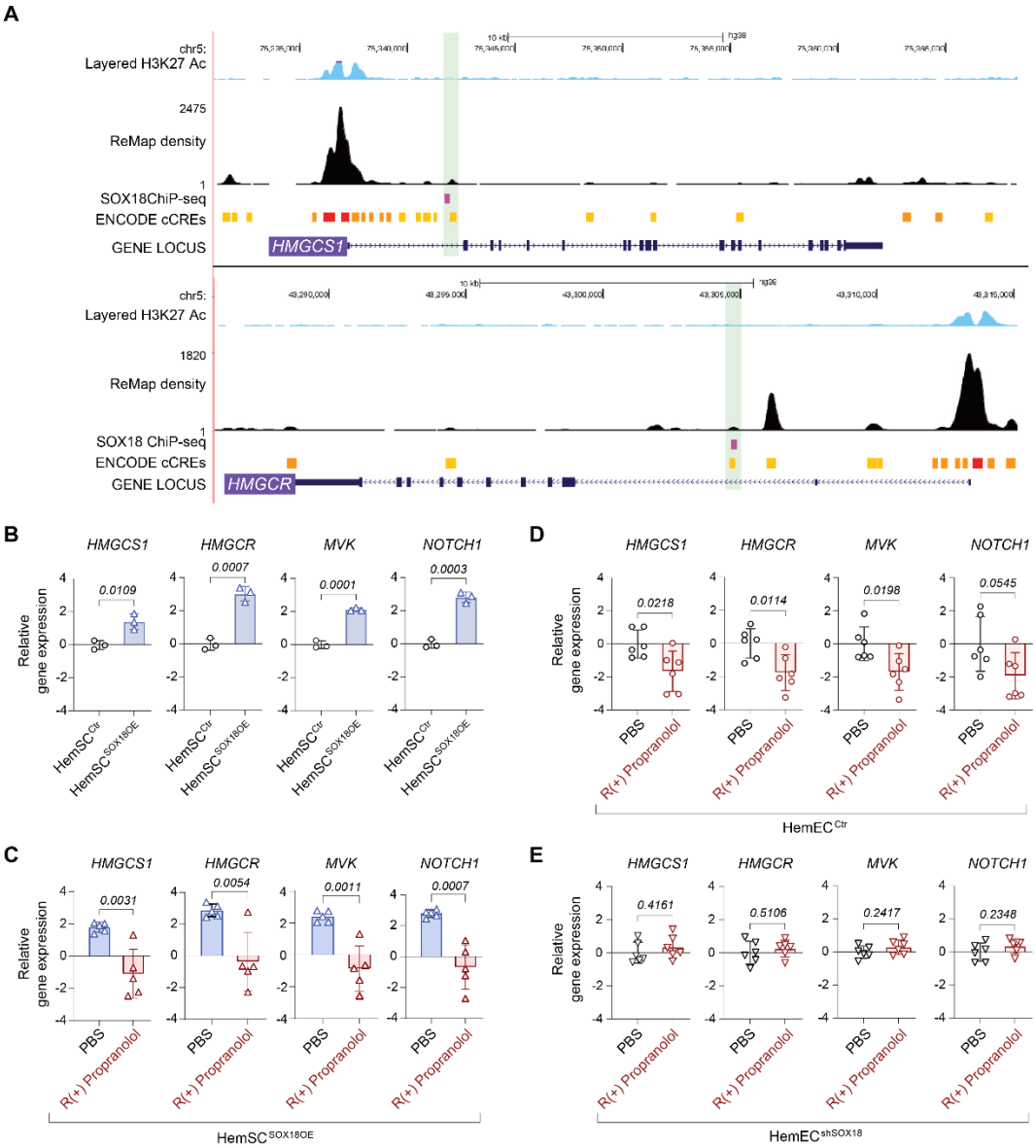

Figure 2. **SOX18 fine tunes endothelial MVP gene expression.** (**A**) ChIP-Seq dataset in HUVEC identifies SOX18 binding sites within the *HMGCS1* and *HMGCR* gene loci. (**B**) Lentiviral SOX18 overexpression in undifferentiated HemSC (HemSC^{SOX18OE}) versus control HemSC (HemSC^{Ctr}). RNA analyzed for *HMGCS1*, *HMGCR*, *MVK,* and *NOTCH1* by qPCR (n=3 independent experiments). (**C**) Treatment of HemSC^{SOX18OE} ± R(+) propranolol for 24 hours (n=5 independent experiments). (**D**) Treatment of IH-derived control HemEC with R(+) propranolol for 24 hours. RNA analyzed for *HMGCS1*, *HMGCR*, *MVK*, and *NOTCH1* by qPCR. (**E**) HemEC with lentiviral knockdown of SOX18 (HemEC ^{shSOX18}) were treated with R(+) propranolol for 24 hours followed by qPCR analyses (n=3 biological replicates, performed in 2 independent experiments yielding n=6 data points; lentiviral knockdown of SOX18 was performed twice in each of the 3 HemEC lines with an efficiency cut-off of >70%). P values were calculated using a two-tailed, unpaired t-test (**B-E**). Data show the mean ± SD.

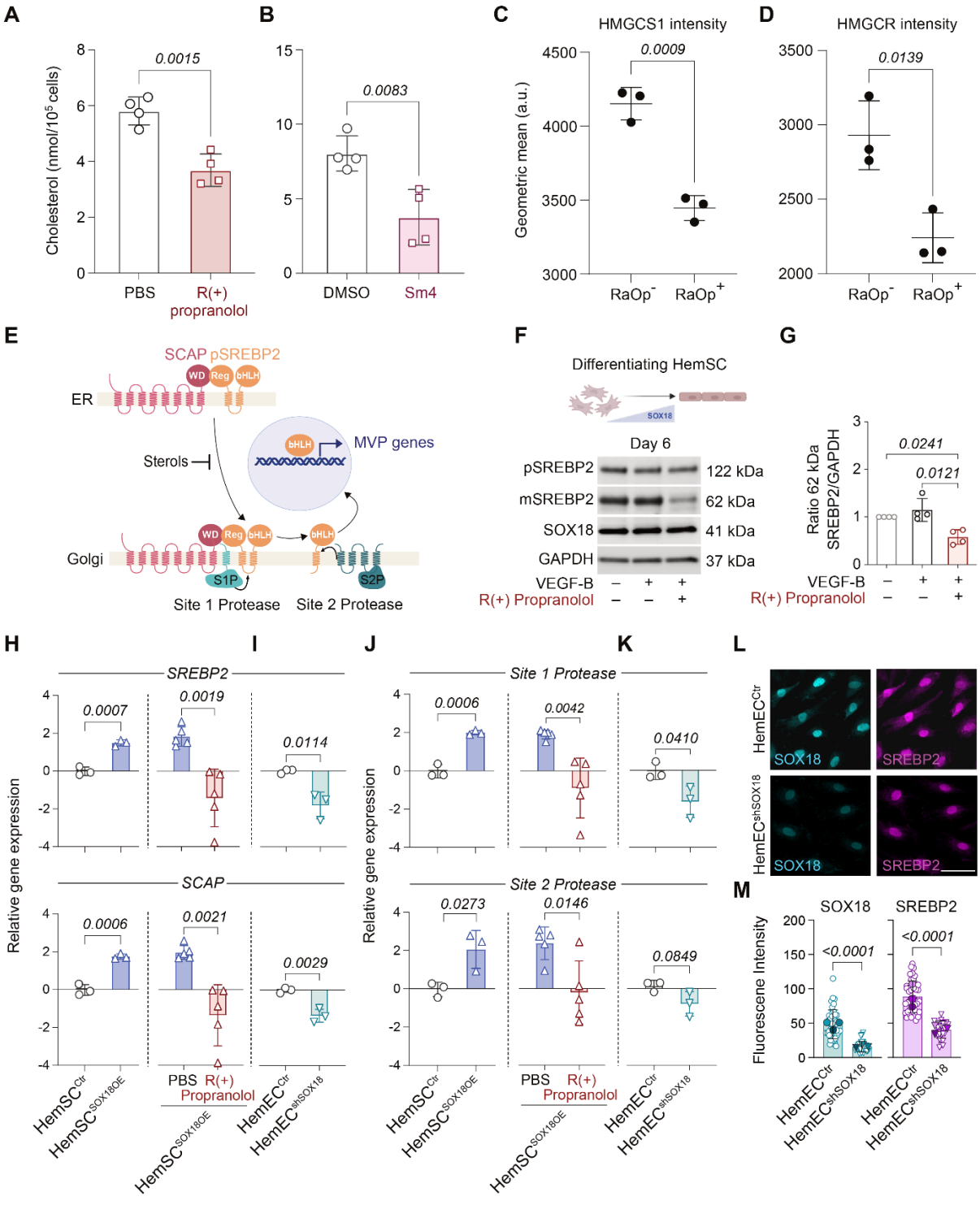

848

849 **Figure 3**. **Biosynthetic output of the MVP is mediated via a SOX18-/SREBP2-dependent mechanism.**
850 (**A**,**B**). HUVECs incubated with MBCD for 16 hours, followed by treatment ± R(+) propranolol or ± Sm4 for
851 16 hours. Endogenous cholesterol levels were measured by mass spectrometry (n=3 biological replicates).
852 (**C**,**D**) Overexpression of Ragged Opossum (*RaOp*) in HUVECs followed by immunofluorescent staining of
853 HMGCS1 and HMGCR (n=3 biological replicates). P values were calculated using a 2-tailed, unpaired t-test

(**A**,**B**) and by a one-way ANOVA multiple comparisons test with Tukey-correction (**C**,**D**). Data show the mean ± SD. (**E**) Schematic of SREBP2 maturation by SCAP, Site 1 protease and Site 2 protease (S1P, S2P) to produce the bHLH domain that translocates to the nucleus. (**F**,**G**) HemSC undergoing endothelial differentiation for 6 days were treated for 2 hours ± R(+) propranolol, lysed, and analyzed by WB with anti-SREBP2, anti-SOX18, and anti-GAPDH (n=3 biological replicates; 1 of the biological replicates analyzed in two independent experiments yielding n=4 data points). (**H**,**K**) Relative gene expression of *SREBP2*, *SCAP*, *S1P*, and *S2P* in $HemSC^{Ctr}$ versus $HemSC^{SOX18OE}$; with $HemSC^{SOX18OE}$ treated ± R(+) propranolol for 24 hours. (**J**,**K**) Relative gene expression of *SREBP2*, *SCAP*, *S1P*, and *S2P* in $HemEC^{Ctr}$ versus $HemEC^{shSOX18}$. (**L**,**M**) Immunofluorescence staining of SOX18 and SREBP2 in $HemEC^{shSOX18}$ versus $HemEC^{Ctr}$ (n=3 biological replicates). Scale bar 25 µm. P values were calculated using a two-tailed, unpaired t-test (**A**-**D**, **H**-**M**) and a one-way ANOVA multiple comparisons test with Šidák-correction (**F**,**G**). Data represent sample sizes n=4 (**A**,**B**) and n=3 (**C**,**D,I**,**K**,**M**) biological replicates, and n=3 biological replicates with 1 of the biological replicates analyzed in two independent experiments yielding n=4 data points (**F**,**G**), n=3-5 independent experiments (**H**,**J**). Data show the mean ± SD.

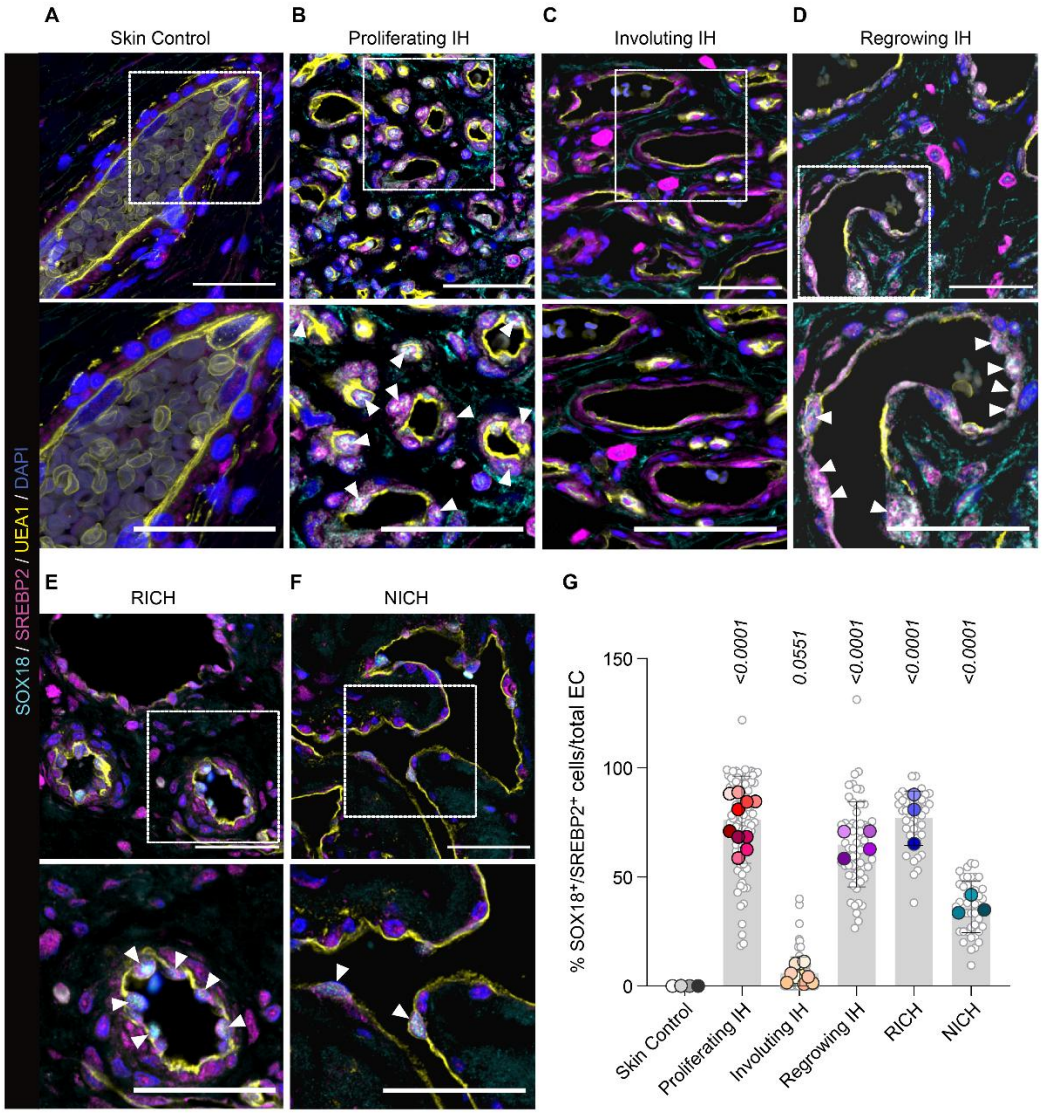

Figure 4. Nuclear co-localization of SOX18 and SREBP2 in IH and congenital vascular tumors. (**A**-**D**) Human age-matched skin, proliferating IH, involuting IH and regrowing IH stained with anti-SREBP2 (magenta), anti-SOX18 (cyan), and the human EC-specific lectin UEA1 (yellow). Cell nuclei stained with DAPI (blue). (**E-F**) Congenital hemangiomas RICH and NICH stained in the same manner. Boxed areas are shown enlarged in the bottom rows. (**G**) $SOX18^{+}/SREBP2^{+}$ double positive cell nuclei (arrowheads) were quantified and expressed relative to total EC. P values were calculated using one-way ANOVA with Šidák-correction. Data show the mean ± SD. Data represent 15 representative images each for patient sample sizes n=4 for age-matched skin controls, n=10 each for proliferating and involuting phase IH, n=4 for regrowing IH, n=3 each for RICH and NICH. See Table 1 for detailed patient information. Scale bars 50 µm (upper panels) and 25 µm (lower magnified panels).

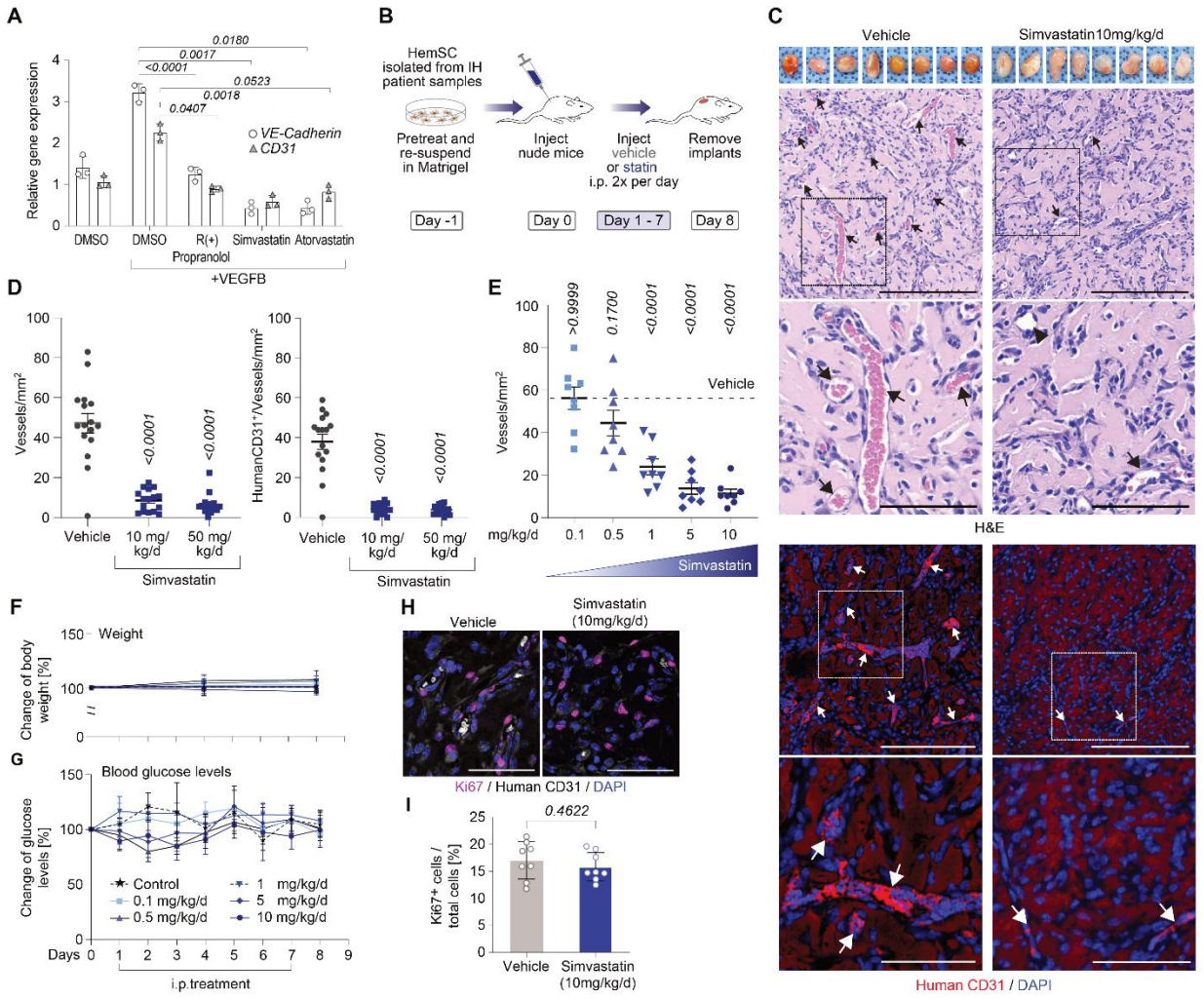

Figure 5. Statins inhibit HemSC endothelial differentiation and blood vessel formation (**A**) HemSC induced to undergo endothelial differentiation for 6 days in the presence of simvastatin (0.5 µM), atorvastatin (0.1 µM), or R(+) propranolol (10 µM) (n=3). VE-Cadherin (open circles) and CD31 (open triangles) measured by qPCR. R(+) propranolol served as positive control. (**B**) Schematic of IH xenograft model. (**C**) Matrigel implants harvested after 7 days shown (top panels) . H&E staining highlights blood vessel lumens with red blood cells (middle panels). Anti-human CD31 staining (red) indicates human blood vessels (bottom panels). Cell nuclei stained with DAPI (blue). Scale bars 100 µm and 50 µm. (**D**) Vessels/mm^2 in H&E-stained sections (left); human CD31+ vessels/mm^2 (right). (**E**) Dose response to simvastatin. (**F**,**G**) Blood glucose levels and body weight of mice over 8 days. (**H**) Immunofluorescent staining for Ki67 and human CD31 in sections from control and simvastatin-treated mice (n=8 biological replicates). Data were from 2 implants per mouse, leading to an observation sample size of n=24 for vehicle (combined), n=14 for 10 mg/kg/d, and n=16 for 50 mg/kg/d simvastatin (**D**), n=10 for vehicle, n=10 for 10 mg/kg/d, n=10 for 5 mg/kg/, n=10 for 1 mg/kg/d, n=10 for 0.5 mg/kg/d, and n=10 for 0.1 mg/kg/d simvastatin in the dose response experiment in (**E**). P values were calculated using one-way ANOVA multiple comparisons test with Tukey-correction (**A**,**D**), one-way ANOVA multiple comparisons test with

916 Dunnett-correction(**E**), two-way ANOVA multiple comparisons test with Dunnett-correction (**F**), and a
917 two-tailed, unpaired t-test (**I**). Data shown as ± SD.

918

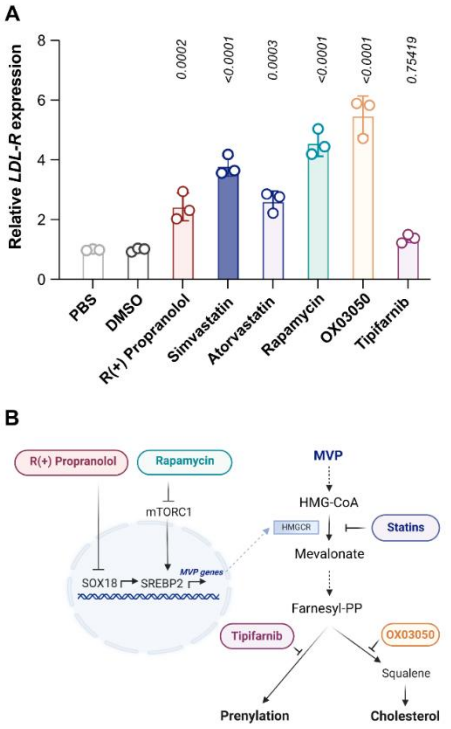

Figure 6

Figure 6: Drug modulation along the SOX18-MVP axis in HemSC results in upregulation of *LDL receptor* mRNA levels. (**A**) *LDL receptor* mRNA was measured in HemSC following 24-hour treatment with 10 µM R(+) Propranolol, 0.5 µM Simvastatin, 0.1 µM Atorvastatin, 20 nM Rapamycin, 28 nM OX03050, a squalene synthase 1 inhibitor, or 0.1 µM of the farnesyltransferase inhibitor tipifarnib. PBS (for R(+) Propranolol) and DMSO (all other drugs) served as vehicle controls. P values were calculated using one-way ANOVA with Šidák-correction. Data show the mean ± SD (n=2 biological replicates; one of the replicates was used in two independent experiments resulting in 3 data points). (**B**) Schematic illustrates points of inhibition of the different drugs along the endothelial SOX18-MVP axis.